13

Assessing the Effect of Large Igneous Provinces on Global Oceanic Redox Conditions Using Non-traditional Metal Isotopes (Molybdenum, Uranium, Thallium)

Brian Kendall[1], Morten B. Andersen[2], and Jeremy D. Owens[3]

ABSTRACT

Large igneous provinces (LIPs) have occurred episodically throughout Earth's history, with the most severe events causing profound disturbances to Earth's climate and biosphere that likely influenced the course of metazoan evolution. One environmental perturbation caused by LIP emplacement is a change in global oceanic redox conditions. The uranium (U) and molybdenum (Mo) isotope systems are relatively established tracers of global oceanic redox conditions, particularly for the extent of anoxic and euxinic seafloor, whereas the thallium (Tl) isotope system is emerging as a tracer for the extent of well-oxygenated seafloor characterized by manganese (Mn) oxide burial. In this review, we discuss how these metal isotope systems can be used to infer changes to global oceanic redox conditions through the cascade of environmental perturbations caused by LIP emplacement, focusing on the three events (Cenomanian-Turonian, Toarcian, and Permian-Triassic) that have received the most attention. Existing isotope mass-balance models for these metals indicate an expansion of oceanic anoxia and euxinia (by ~1 to 2 orders of magnitude greater than the modern ocean) accompanied LIP emplacement during these events. Future studies, ideally utilizing a multi-isotope approach on the same samples and coupled with improvements in oceanic metal isotope mass balances and modeling, are expected to provide more precise and accurate estimates of the spatiotemporal extent of oceanic anoxia/euxinia expansion and how this relates to the magnitude, location, and style of LIP events.

13.1. INTRODUCTION

During the past two decades, the isotope ratios of numerous redox-sensitive metals in sedimentary archives (particularly organic-rich mudrocks, carbonates, and iron formations) have emerged as valuable tools for constraining changes in global oceanic redox conditions. The long modern ocean residence times of Mo (~440 kyr; Miller et al., 2011), U (~450 kyr; Dunk et al., 2002), and Tl (~20 kyr; Nielsen et al., 2017) relative to ocean mixing times (~1–2 kyr; Sarmiento & Gruber, 2006), together with the distinctive isotope fractionations observed for metal removal into diverse marine sinks, means that the isotopic composition of these metals can serve as global oceanic redox tracers. Redox-sensitive metal isotopes have become an attractive tool with which to place constraints on the magnitude of oceanic anoxia associated with the emplacement of LIPs. The overarching approach is to use sedimentary rocks (organic-rich mudrocks for Mo, U, and Tl; carbonates for U) to infer the isotopic composition of coeval global seawater before, during, and after LIP emplacement, and employ isotopic mass

[1] *Department of Earth and Environmental Sciences, University of Waterloo, Waterloo, Ontario, Canada*

[2] *School of Earth and Ocean Sciences, Cardiff University, Cardiff, UK*

[3] *Department of Earth, Ocean and Atmospheric Science and National High Magnet Field Laboratory, Florida State University, Tallahassee, Florida, USA*

Large Igneous Provinces: A Driver of Global Environmental and Biotic Changes, Geophysical Monograph 255, First Edition.
Edited by Richard E. Ernst, Alexander J. Dickson, and Andrey Bekker.

DOI: 10.1002/9781119507444.ch13

balance models to link and infer changes in the global extent of seafloor covered by oxic versus anoxic (euxinic and noneuxinic) waters. For ancient LIP events with negligible open-ocean seafloor records, changes in global oceanic redox conditions must be inferred from the metal isotope ratios of continental margin sedimentary rocks.

Differences in marine input/output fluxes, ocean residence times, and isotope fractionation mechanisms for Mo, U, and Tl mean that each metal provides its own perspective on changes in oceanic redox conditions during LIP emplacement. Because Mo is highly insoluble in sulfidic environments and is thus enriched in euxinic sediments (Helz et al., 1996; Erickson & Helz, 2000; Scott & Lyons, 2012), Mo isotope data from euxinic organic-rich mudrocks are typically used to infer the global extent of seafloor where dissolved sulfide occurs in the water column and sediments (e.g., Arnold et al., 2004; Dahl et al., 2011; Goldberg et al., 2016). Uranium is insoluble in its reduced form and, in contrast to Mo, does not require dissolved sulfide for its incorporation and burial into sediments (Morford & Emerson, 1999; Algeo & Tribovillard, 2009). Despite this geochemical difference, it is not fully clear if U isotopes are best used as a tracer for the global extent of general oceanic anoxia (euxinic and noneuxinic) or more specifically the global extent of oceanic euxinia because of knowledge gaps for isotope fractionation factors and U removal mechanisms in anoxic marine environments (Stylo et al., 2015; Hood et al., 2016; Andersen et al., 2017; Brown et al., 2018; Cole et al., 2020). Nevertheless, U isotope data from organic-rich mudrocks and carbonates have gained prominence as a tool for tracing global oceanic redox changes during Phanerozoic anoxic events. Thallium isotope compositions from euxinic organic-rich mudrocks have been used to infer the extent of well-oxygenated seafloor because Tl adsorption to Mn oxides in oxygenated settings is associated with the largest known marine Tl isotope fractionation (Nielsen et al., 2011; Peacock & Moon, 2012; Owens et al., 2017a). The lower ocean residence time of Tl and the sensitivity of this metal's oceanic mass balance to Mn oxide burial fluxes means that the seawater isotopic composition of Tl will respond faster than Mo or U to regional/global ocean deoxygenation at the onset of Phanerozoic anoxic events (Ostrander et al., 2017; Them et al., 2018).

This chapter first reviews the modern oceanic mass balance for these three isotope systems (Fig. 13.1; see Table 13.1 for data reporting conventions). Application of these isotope systems as tracers for global oceanic redox changes during major Phanerozoic LIP events is then discussed. Future utilization will ultimately include multiple isotope systems on time equivalent rocks to decipher a holistic global redox structure as related to LIP events and their climatic consequences.

13.2. REDOX-SENSITIVE METAL ISOTOPE SYSTEMS AS GLOBAL OCEANIC REDOX PROXIES

13.2.1. Molybdenum Isotopes

The use of Mo isotopes as an oceanic redox proxy exploits its bimodal redox behavior (+6 and +4 valences; Barling et al., 2001). Molybdate (MoO_4^{2-}) is soluble in oxygenated river water and seawater but is converted to particle-reactive thiomolybdates ($MoO_{4-x}S_x^{2-}$) and polysulfides and removed to sediments in modern sulfidic settings (Collier, 1985; Erickson & Helz, 2000; Scott & Lyons, 2012; Dahl et al., 2013, 2017; Helz & Vorlicek, 2019).

Oceanic Mo inputs are dominated by dissolved riverine and groundwater Mo (>90%), which has an average δ^{98}Mo similar to the upper crust average of ~0.3–0.6‰ (Table 13.1 defines δ-notation; Archer & Vance, 2008; Willbold & Elliott, 2017; King & Pett-Ridge, 2018; Neely et al., 2018). Seafloor hydrothermal systems may constitute a minor dissolved Mo source but its δ^{98}Mo is poorly constrained (Wheat et al., 2002; Reinhard et al., 2013; Neely et al., 2018).

Oceanic Mo outputs are divided into oxic, sulfidic-at-depth (weakly oxic or anoxic bottom waters; dissolved sulfide confined to sediment pore-waters), and euxinic settings that make up ~30% to 50%, ~50% to 65%, and ~5% to 15% of the modern dissolved oceanic Mo input flux, respectively (Fig. 13.1a; Scott et al., 2008; Reinhard et al., 2013). On average, the Mo burial flux in modern euxinic environments not severely restricted from the open ocean (i.e., excluding the Black Sea) is ~1 and ~3 orders of magnitude higher than sulfidic-at-depth and oxic settings, respectively (Scott et al., 2008; Reinhard et al., 2013). Comparing the magnitude of these sinks with their areal seafloor extent (~2% for sulfidic-at-depth and ~0.1% for euxinic; Reinhard et al., 2013) reveals that the oceanic Mo mass balance is highly sensitive to the extent of sulfidic (especially euxinic) environments. Hence, seawater Mo concentrations and residence times will be lower in ancient oceans with a greater extent of euxinic seafloor than today (Reinhard et al., 2013).

In all marine settings, Mo isotope fractionation results in preferential removal of light Mo isotopes to sediments. The largest Mo isotope fractionation ($\Delta^{98}Mo_{seawater\text{-}sediment}$ ~3‰) occurs in well-oxygenated settings where Mo adsorbs to Mn oxides (Siebert et al., 2003; Barling & Anbar, 2004; Wasylenki et al., 2008). In sulfidic-at-depth environments, Mo isotope fractionation is variable and depends on the type of (oxyhydr)oxides delivering Mo to sediments and pore-water H_2S content, with Mo burial most efficient when pore-waters have high dissolved sulfide (average fractionation of ~0.7–0.9‰; Poulson et al., 2006; Siebert et al., 2006; Poulson Brucker

(a) $\delta^{98}Mo$

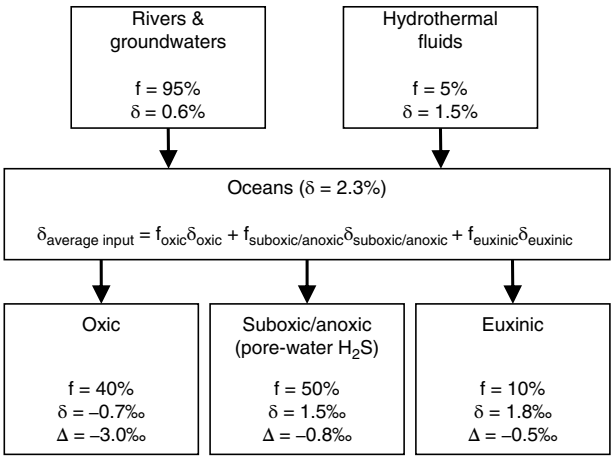

(b) $\delta^{238}U$

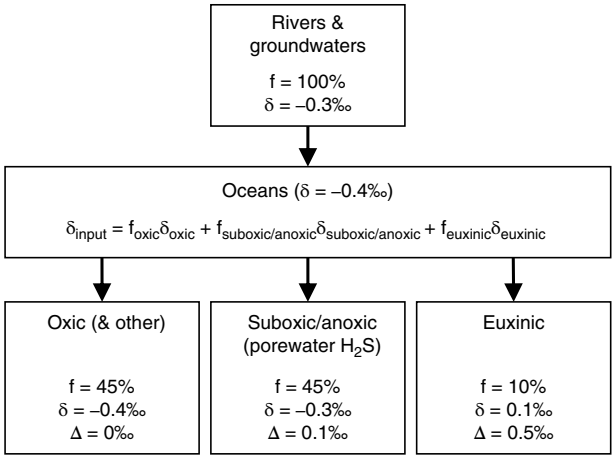

(c) $\varepsilon^{205}T1$

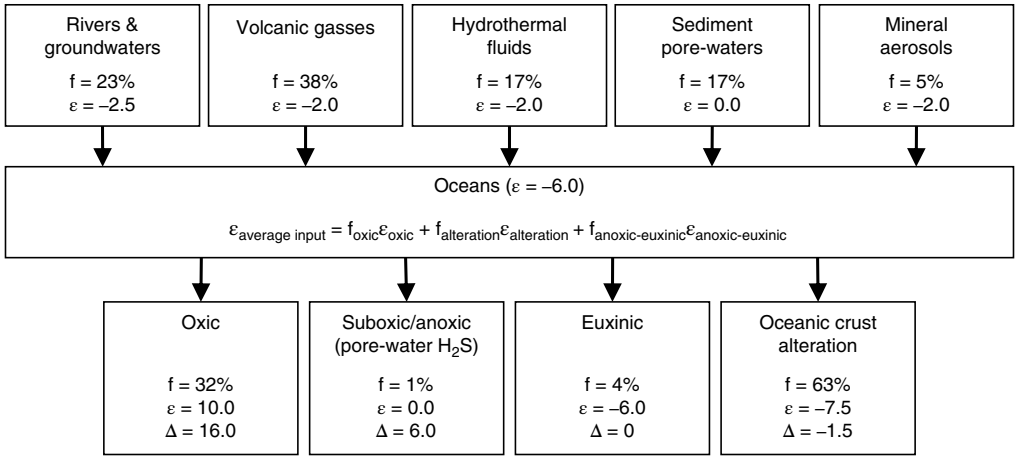

Figure 13.1 Approximate global oceanic isotope mass balance of (a) Mo, (b) U, and (c) Tl for the modern ocean, assuming steady-state conditions. For each metal, relevant fluxes are expressed as a percentage of total input or output and the average isotopic composition (δ or ε values) and isotopic fractionation ($\Delta_{sediment-seawater}$) of each flux is given. For molybdenum, the isotopic composition of the hydrothermal flux is poorly constrained and the value shown (1.5‰) enables mass balance to be achieved. For uranium, the "oxic and other" sink includes Mn oxides, carbonates, pelagic sediments, coastal sediments, and alteration of oceanic crust. This particular mass balance for U takes into account the possibility that U burial in anoxic/noneuxinic settings (i.e., dissolved H_2S confined to pore-waters) is typically associated with a smaller U isotope fractionation than euxinic settings (Hood et al., 2016; Cole et al., 2020). Other mass-balance models have assumed a large U isotope fractionation in all anoxic environments (euxinic and noneuxinic) (Tissot & Dauphas, 2015; Andersen et al., 2016; Noordmann et al., 2016). Further studies are needed to constrain the average U isotope fractionation for anoxic/noneuxinic settings. For thallium, the mass-balance model places suboxic and anoxic into a single sedimentary sink (whose isotopic fractionation is based on limited data and requires more systematic study) and includes euxinic sediments as a separate sink that captures the seawater isotope composition. See text for references.

Table 13.1 Data Reporting Conventions for the Mo, U, and Tl Isotope Systems

Isotope system	Convention	Standard
Molybdenum	$\delta^{98}Mo\ (‰) = 10^3 \times [(^{98}Mo/^{95}Mo)_{sample} / (^{98}Mo/^{95}Mo)_{standard}) - 1] + 0.25$	NIST SRM 3134
Uranium	$\delta^{238}U\ (‰) = 10^3 \times [(^{238}U/^{235}U_{sample}) / (^{238}U/^{235}U_{standard}) - 1]$	CRM 145
Thallium	$\varepsilon^{205}Tl = 10^4 \times [(^{205}Tl/^{203}Tl_{sample}) / (^{205}Tl/^{203}Tl_{standard}) - 1]$	NIST SRM 997

Source: Reviewed in Andersen et al. (2017), Kendall et al. (2017), Nielsen et al. (2017).

et al., 2009, 2012; Goldberg et al., 2012). In euxinic settings, Mo isotope fractionation is <0.3–3‰. Larger fractionations reflect weakly/intermittently euxinic conditions and/or a strong Fe-Mn (oxyhydr)oxide particulate flux that delivers isotopically light Mo to sediments (Arnold et al., 2004; Neubert et al., 2008; Nägler et al., 2011; Noordmann et al., 2015; Andersen et al., 2018; Bura-Nakić et al., 2018; Scholz et al., 2018). The $\delta^{98}Mo$ of euxinic sediments approaches seawater $\delta^{98}Mo$ when Mo removal from bottom waters is near quantitative, particularly in significantly restricted (but not isolated) basins with water stratification and highly sulfidic ($[H_2S]_{aq}$ >11 μM) bottom waters (e.g., Black Sea; Barling et al., 2001; Arnold et al., 2004; Neubert et al., 2008).

The decrease in Mo isotope fractionation from well-oxygenated to strongly euxinic environments requires that global seawater $\delta^{98}Mo$ (2.34 ± 0.10‰ today; Nakagawa et al. 2012; Nägler et al., 2014) is influenced by global oceanic redox conditions, particularly the extent of euxinic seafloor where sedimentary Mo burial rates are high. In a well-oxygenated ocean, the strong preferential removal of lighter Mo isotopes to Mn oxides drives global seawater to high $\delta^{98}Mo$. By contrast, an expansion of euxinic (and sulfidic-at-depth) settings will cause global seawater $\delta^{98}Mo$ to decrease and be closer to the oceanic input $\delta^{98}Mo$ (Fig. 13.2; Barling et al., 2001; Arnold et al., 2004). Organic-rich mudrocks deposited from locally euxinic waters are the main sedimentary archive used to infer changes in global seawater $\delta^{98}Mo$.

Understanding global oceanic redox changes during LIP events requires knowledge of oceanic input $\delta^{98}Mo$. Global riverine $\delta^{98}Mo$ probably has not varied significantly during the Phanerozoic (Kendall et al., 2017). Hydrothermal fluids, which play a minor role in the modern oceanic Mo budget, may have been more important during LIP events but it is not known if hydrothermal

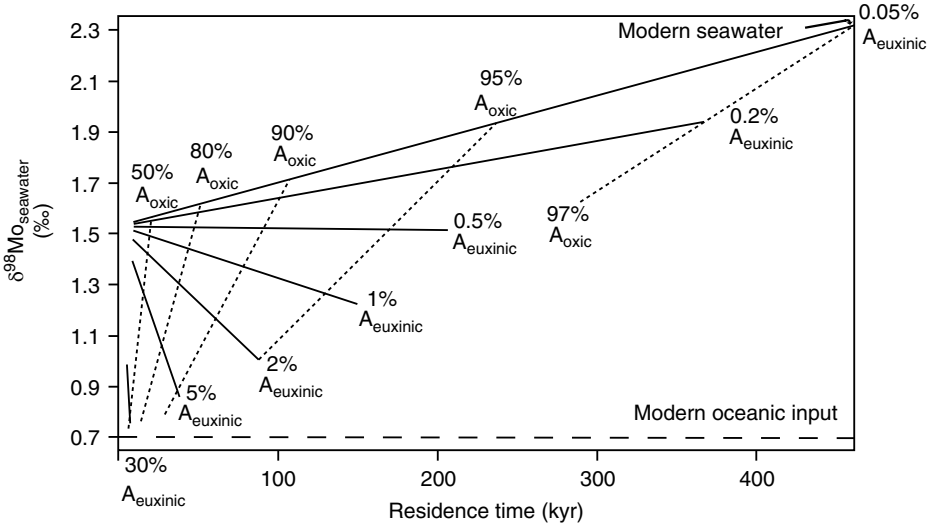

Figure 13.2 Mass-balance model solutions for the areal extent of seafloor covered by oxic and euxinic waters with respect to seawater $\delta^{98}Mo$ and oceanic Mo residence time (modified from Goldberg et al., 2016). Calculated residence times are likely underestimated because the assumed Mo burial rates for the oceanic sinks rely heavily on data from modern continental margin environments (burial rates should be lower for open-ocean abyssal sediments). Dotted lines denote the areal extent of oxic seafloor; solid lines denote the areal extent of euxinic seafloor. Suboxic and anoxic environments with dissolved H_2S restricted to sediment pore-waters (sulfidic-at-depth) are not shown (to retain clarity) and can be calculated as $A_{suboxic\text{-}anoxic}\ (\%) = 100 - A_{oxic} - A_{euxinic}$. As the extent of oxic seafloor (with lower Mo burial rates) contracts and euxinic seafloor (with higher Mo burial rates) expands, both the seawater $\delta^{98}Mo$ and oceanic Mo residence time decrease. For seawater $\delta^{98}Mo$ = 1.4‰ and 0.8‰, $A_{euxinic}$ is likely <5% and >5%, respectively. See Goldberg et al. (2016) for a detailed mathematical description of the mass-balance model.

fluid δ^{98}Mo is sufficiently different from rivers/groundwaters to significantly impact the oceanic Mo isotope budget (Wheat et al., 2002; Neely et al., 2018). Subaerial weathering of mafic igneous rocks probably does not substantially change oceanic input δ^{98}Mo because such rocks have only slightly lower δ^{98}Mo than the more felsic upper continental crust (Yang et al., 2015; Willbold & Elliot, 2017).

13.2.2. Uranium Isotopes

The utility of U isotopes as an oceanic redox proxy is related to U^{6+} and U^{4+} redox exchange in surface environments and associated isotope fractionation between the two long-lived radioactive isotopes ^{238}U and ^{235}U (Stirling et al., 2007; Weyer et al., 2008).

Oxygenated open-ocean seawater is dominated by dissolved U^{6+} (associated with carbonate complexes) and is characterized by invariant $\delta^{238}U = -0.39 \pm 0.02$‰ (Andersen et al., 2014; Tissot & Dauphas, 2015). The seawater δ^{238}U value is lower than the average δ^{238}U for the continental crust, mantle, and dissolved riverine flux (δ^{238}U ~–0.30‰; Tissot & Dauphas, 2015; Andersen et al., 2016, 2017), the latter constituting the main oceanic input (Dunk et al., 2002). Marine U sinks consist, in order of largest to smallest flux, of reducing sediments (euxinic, anoxic/non-euxinic, hypoxic), carbonates, low-temperature hydrothermal alteration of mafic oceanic crust, and adsorption to pelagic clays and Fe-Mn deposits (Fig. 13.1b; Dunk et al., 2002; Tissot & Dauphas, 2015). Both modern reducing sediments and altered oceanic crust are, on average, isotopically heavier than seawater (δ^{238}U ~–0.3‰ to +0.2‰) because they dominantly sequester reduced U^{4+} (Weyer et al., 2008; Andersen et al., 2014, 2015; Holmden et al., 2015; Noordmann et al., 2015; Bura-Nakić et al., 2018). Carbonate deposits are generally either unfractionated or isotopically heavier than seawater (δ^{238}U ~–0.4 to 0.1‰) depending on the amount of U uptake from reducing pore-waters (Romaniello et al., 2013; Chen et al., 2018; Tissot et al., 2018). On the other hand, oxic sediments, represented by Fe-Mn crusts, are isotopically light relative to seawater (δ^{238}U ~–0.6 ‰; Weyer et al., 2008; Goto et al., 2014; Wang et al., 2016a), consistent with experiments on U adsorption to Mn oxides (Brennecka et al., 2011a).

The different direction of isotopic fractionation of oxic and reducing marine U sinks provides a proxy to reconstruct the redox conditions of ancient oceans and thus changes in global oceanic redox conditions through time, using similar principles as described for the Mo isotope proxy in section 13.2.1. An expansion of oceanic euxinia will cause an increase in the areal extent of seafloor where the heavier ^{238}U is preferentially removed to organic-rich sediments, thus causing the global seawater δ^{238}U to decrease. Effects of LIP activity in the form of increased weathering of mafic igneous rocks, hydrothermal fluids, and volcanic outgassing are not expected to appreciably change the oceanic input δ^{238}U because extrusive and intrusive igneous rocks of felsic and mafic composition have similar δ^{238}U (Tissot & Dauphas, 2015).

Organic-rich mudrocks and carbonates have mainly been used as sedimentary archives to infer ancient seawater δ^{238}U after applying a correction for local U isotope fractionation between seawater and sediment during deposition and diagenesis. These estimates of ancient seawater δ^{238}U have inherent uncertainties because the magnitude of local isotope fractionation between seawater and sediments depends on multiple depositional/diagenetic factors, including bottom water and sediment-pore water redox conditions, eustatic sea-level variations, extent of local basin restriction from the open ocean, sedimentation rates, and depositional setting (shallow platform to deep basin floor) (e.g., Romaniello et al., 2013; Andersen et al., 2016; Chen et al., 2018; Clarkson et al., 2018; Bura-Nakić et al., 2018; Tissot et al., 2018). Near-quantitative removal of U from bottom waters will lead to organic-rich sediments preserving near-seawater δ^{238}U compositions (Kyllaren Fjord and Lake Rogoznica) (Noordmann et al., 2015; Bura-Nakić et al., 2018), but nonquantitative U removal results in sediment δ^{238}U being ~0.4–0.6‰ higher than global seawater (Black Sea, Cariaco Basin, Saanich Inlet) (Weyer et al., 2008; Montoya-Pino et al., 2010; Andersen et al., 2014; Holmden et al., 2015; Rolison et al., 2017). Significant variability in seawater-sediment U isotope fractionation also occurs during deposition and diagenesis of shallow marine carbonates, such that carbonate δ^{238}U of ~0.2–0.4‰ above global seawater δ^{238}U are common (Chen et al., 2018; Tissot et al., 2018). Deep-water pelagic foraminiferal-nannofossil carbonates may better capture global seawater δ^{238}U but this may not occur if shallow platform carbonate sediment was transported downslope and mixed with pelagic sediment (Clarkson et al., 2018; Tissot et al., 2018).

13.2.3. Thallium Isotopes

The utilization of Tl as a low-temperature ocean redox proxy is relatively new (Nielsen al., 2009; 2011; Owens et al., 2017a) although the modern oceanic mass balance framework is relatively well constrained (Rehkämper et al., 2002, 2004; Rehkämper & Nielsen, 2004; Nielsen et al., 2005, 2006a, 2017; Baker et al., 2009; Owens et al., 2017a). Thallium exists in two valence states (+1 and +3). In modern surface settings, the redox state of Tl is predominately +1 but is oxidized to +3 by surface oxidation when adsorbed onto hydrogenous low-temperature Mn oxides, specifically birnessite (Bidoglio et al., 1993; Peacock & Moon, 2012; Nielsen et al., 2013).

There are five constrained fluxes of Tl into the oceans, namely volcanic gasses, rivers, hydrothermal fluids, sediment pore-waters, and mineral aerosols (e.g., dust). Importantly, the isotopic values of these inputs are all close to the bulk mantle ε^{205}Tl value of –2 ε-units (Fig. 13.1c; Table 13.1 defines ε-notation; Nielsen et al., 2006b, 2015, 2017). Thus, changes in inputs likely do not drive major shifts in global seawater ε^{205}Tl (–6 for the modern ocean; Rehkämper et al., 2002; Rehkämper & Nielsen, 2004; Nielsen et al., 2006a; Owens et al., 2017a) but can alter the ocean residence time of Tl. Volcanic gasses, hydrothermal fluids, and aerosols constitute ~60% of the input flux and each reservoir has an average isotopic value of –2 with little variation (Nielsen et al., 2006a, 2017; Baker et al., 2009). Riverine input constitutes ~25% and has an average isotopic value of –2.5 (Rehkämper & Nielsen, 2004; Nielsen et al., 2005). The remaining ~15% of inputs are from sediment pore fluids (likely partially related to redox reactions where sedimentary Mn oxides are dissolved in low-O_2 conditions) that have an average ε^{205}Tl of 0 but encompass a larger range of values (Rehkämper & Nielsen 2004; Nielsen et al., 2017).

Dissolved Tl fluxes out of the ocean are dominated by two major sinks: low-temperature alteration of oceanic crust (AOC) and adsorption to Mn oxides (Nielsen et al., 2017). These two sinks are estimated to sequester ~95% of the oceanic Tl inventory (Owens et al., 2017a). Low-temperature AOC is the larger of these two sinks, removing ~65% of all oceanic Tl, and is estimated to have an average ε^{205}Tl of ~–1.5 lower than the seawater value (Owens et al., 2017a). There is a large isotope fractionation associated with burial of adsorbed Tl onto Mn oxides, specifically birnessite (Bidoglio et al., 1993; Peacock & Moon, 2012; Nielsen et al., 2013), which has an isotopic fractionation from modern seawater of ~+16 (Rehkämper & Nielsen, 2004; Rehkämper et al., 2004; Nielsen et al., 2017; Owens et al., 2017a). Suboxic/anoxic and euxinic sediments are minor Tl sinks. Sediments from the two largest modern euxinic basins, the Black Sea and Cariaco Basin, record (within analytical uncertainty) the oxic shallow seawater ε^{205}Tl in those basins (Owens et al., 2017a), with Tl held predominantly in pyrite (Nielsen et al., 2011). The less restricted Cariaco Basin sediments have ε^{205}Tl similar to South Atlantic seawater, whereas the more restricted Black Sea sediments do not capture open-ocean seawater ε^{205}Tl (Owens et al., 2017a). Limited data from oxygen minimum zones with reducing, noneuxinic sediments suggest a range of Tl isotope values (Nielsen et al., 2011) that is likely due to Mn oxide reduction near sulfidic pore fluids. However, in some cases, sediments from such settings may capture seawater values (Fan et al., 2020).

The relatively straightforward isotopic mass balance for Tl and the ability of organic-rich mudrocks deposited in less-restricted basins to record the global open ocean ε^{205}Tl allows for deep-time seawater reconstructions (Nielsen et al., 2011; Ostrander et al., 2017; Them et al., 2018). For short-term climatic events, variations in the marine Tl isotope record, as obtained from euxinic sediments, can provide vital information about changes in the global burial of Mn oxides, an important proxy given that Mn is one of the first elements to respond to changes in the availability of free O_2 (Rue et al., 1997). Thus, Tl isotopes can potentially respond more quickly to climatic perturbations than Mo and U isotopes to changes in oceanic redox conditions especially given the shorter modern Tl residence time. LIP activity (weathering of mafic igneous rocks, hydrothermal fluids, volcanic outgassing) does not influence the oceanic Tl isotope budget; instead, Tl isotopes likely respond to the associated climatic feedbacks (Ostrander et al., 2017; Them et al., 2018).

13.3. APPLICATION TO PHANEROZOIC LIPS

In this section, we synthesize available knowledge regarding changes in global oceanic redox conditions associated with three LIP events from the perspective of Mo, U, and Tl isotopes (Fig. 13.3). Only one major LIP episode, the Cenomanian-Turonian event, has been studied using all three isotope systems and is discussed first. Subsequently, global oceanic redox changes associated with the Toarcian (Mo-Tl) and end-Permian (U-Mo) LIP events are reviewed. Other LIP events that have received significantly less attention and are not covered here include the Paleocene-Eocene Thermal Maximum (~56 Ma, North Atlantic LIP, Mo isotopes; Dickson et al., 2012), end-Triassic (~202 Ma, Central Atlantic Magmatic Province, U isotopes; Jost et al., 2017), and Frasnian-Famennian (~372 Ma, Viluy LIP, U isotopes; Song et al., 2017; White et al., 2018).

13.3.1. Cenomanian-Turonian (Oceanic Anoxic Event 2, OAE2; ~94 Ma)

The Mo, U, and Tl isotope ratios of organic-rich mudrocks, as well as U isotope ratios from carbonates, have been used to track the expansion of oceanic anoxia and euxinia before and during OAE2 (marked by a positive carbon isotope excursion; CIE) in response to one or more magmatic pulses associated with the Madagascar, High Arctic, and/or Caribbean LIPs.

Changes in the extent of euxinic seafloor across OAE2 were inferred using the Mo isotope compositions of organic-rich mudrocks from multiple sections within the proto-North Atlantic and western Tethys oceans (Westermann et al., 2014; Dickson et al., 2016a; Goldberg et al., 2016; Dickson et al., 2017). Elemental data (sedimentary Fe speciation or Mo/U ratios), biomarkers, and

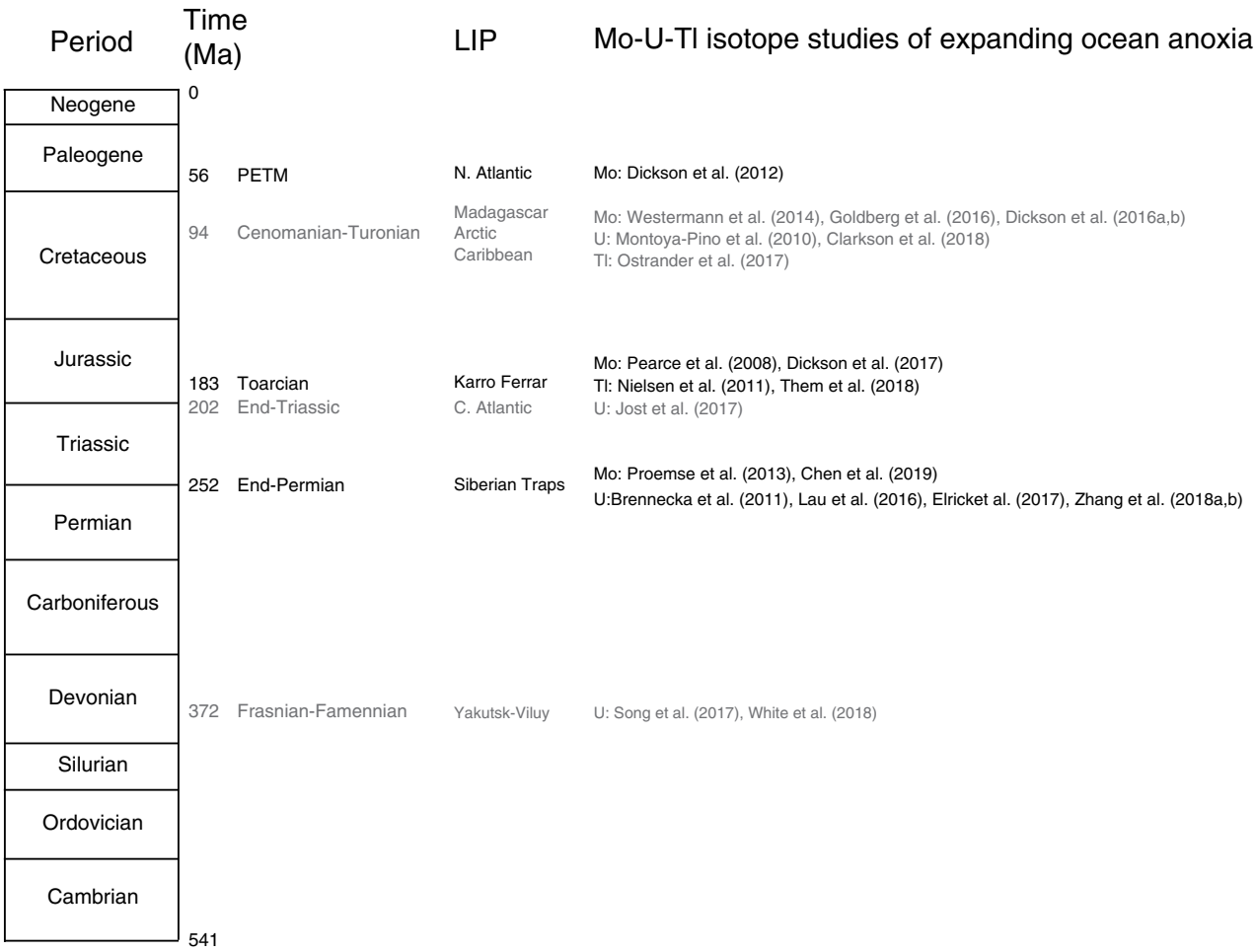

Figure 13.3 Overview of Phanerozoic LIP events that have been studied to infer global oceanic redox changes based on the metal isotope systems of Mo, U, and Tl. PETM = Paleocene-Eocene Thermal Maximum.

absence of benthic fossils suggest anoxic and at least intermittently euxinic conditions for the more restricted Cape Verde Basin in the southern proto-North Atlantic Ocean. This section was considered more likely to capture coeval global seawater δ^{98}Mo than the more open-ocean and noneuxinic Tethyan sections (Westermann et al., 2014; Dickson et al., 2016a).

In the Cape Verde section, the onset of OAE2 is marked by a shift to higher δ^{98}Mo in the mudrocks (Fig. 13.4a). This stratigraphic change is not the expected response to a global expansion of oceanic euxinia, which should decrease global seawater δ^{98}Mo. The increase in δ^{98}Mo and Mo concentrations of the mudrocks at the onset of OAE2 indicates that the development of more reducing conditions locally in the Cape Verde Basin exerted a greater control on sedimentary δ^{98}Mo than global redox change. Within the OAE2 interval, stratigraphic variations in the δ^{98}Mo of euxinic mudrocks occur. These variations can be caused by local changes in bottom-water sulfide concentrations, the efficiency of Mo removal from those bottom waters, and the extent to which an Fe-Mn particulate shuttle delivered isotopically light Mo to sediments (Dickson et al., 2016a). Although Fe speciation and Mo/U ratios can identify locally euxinic conditions, these proxies cannot fingerprint the presence/absence of Mo isotope fractionation between euxinic sediments and seawater. Hence, a conservative approach is to assume the highest δ^{98}Mo of the mudrocks most closely approximates global seawater δ^{98}Mo during OAE2. Using this conservative approach, the Cape Verde data suggest a global seawater δ^{98}Mo of ~1.4‰ at the onset of the global increase in organic carbon burial marked by the start of the positive CIE. As the inferred OAE2 seawater δ^{98}Mo is lower than modern global seawater (2.3‰), this observation is consistent with an expansion of oceanic euxinia in response to LIP emplacement (although LIP activity has been suggested to occur slightly before the CIE; Du Vivier et al., 2015). Mass-balance modeling suggests that euxinic environments made up <5% of the seafloor for a global seawater δ^{98}Mo of ~1.4‰ (Fig. 13.2; Westermann

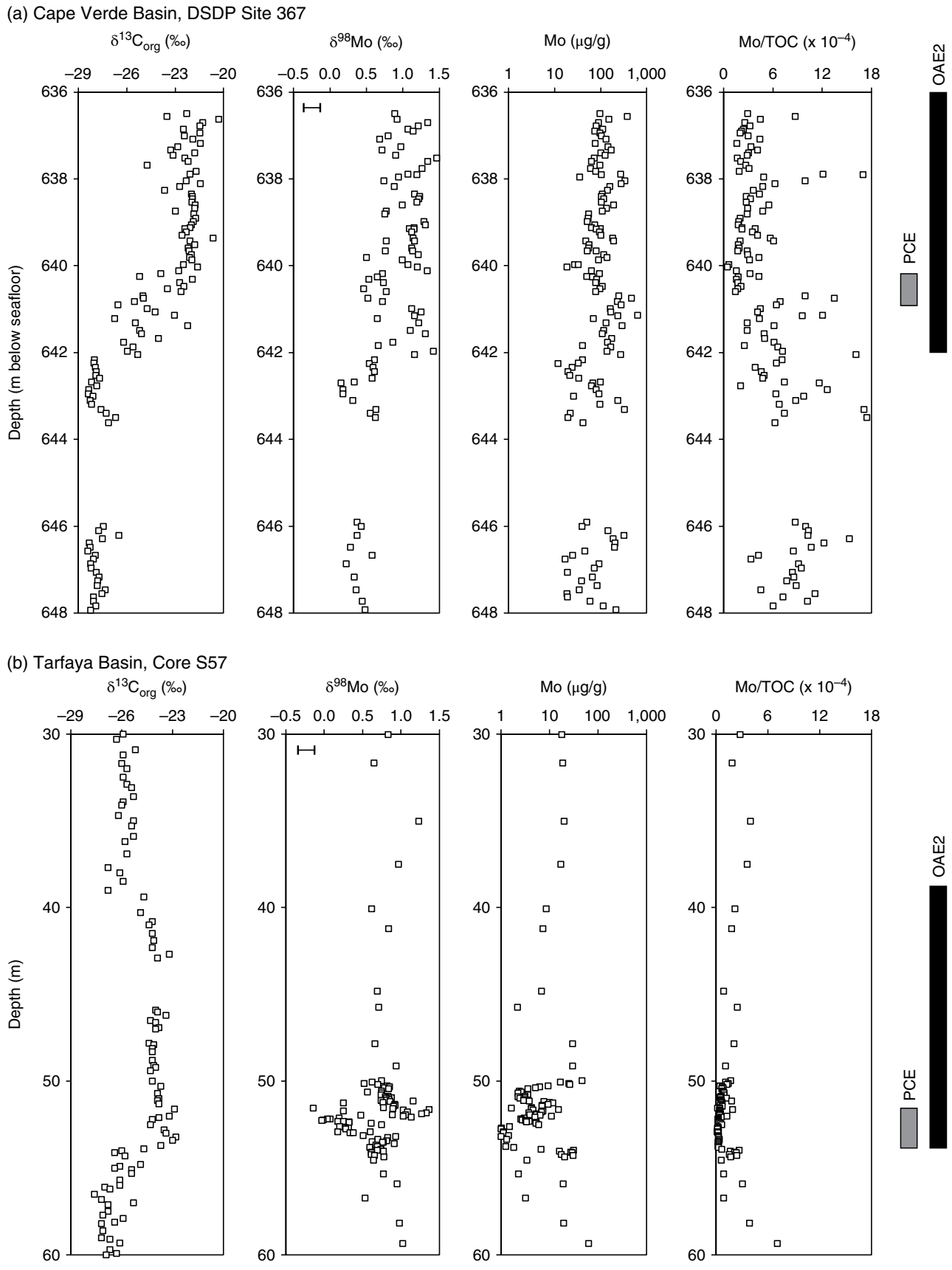

Figure 13.4 Molybdenum concentration and molybdenum isotope data (bulk sample digestions using HF-HNO_3-HCl) for organic-rich mudrocks from (a) DSDP Site 367, Cape Verde Basin (the end of OAE2 is not captured in this section), and (b) Core S57, Tarfaya Basin, across Oceanic Anoxic Event 2 (OAE2). The positive organic carbon isotope excursion marking OAE2 is shown for comparison. All δ^{98}Mo values were renormalized to NIST SRM 3134 = 0.25‰. Typical external 2SD reproducibility of Mo isotope data is ~0.1‰ and is shown by the error bar in both Mo isotope profiles. PCE = Plenus Cold Event (two discrete intervals for this event have been delineated using paleontological and geochemical data, but for simplicity a single grey bar is used to denote the event). TOC = total organic carbon. Data from Westermann et al. (2014), Dickson et al. (2016a), and Goldberg et al. (2016).

et al., 2014; Dickson et al., 2016a; Goldberg et al., 2016), which is in good agreement with estimates derived from S isotopes and Mo concentrations (Owens et al., 2013, 2016; Dickson et al., 2016b).

Subsequently, an excursion to lower δ^{98}Mo occurs in euxinic mudrocks deposited during the Plenus Cold Event (PCE) early during OAE2. This excursion probably does not reflect a change in global seawater δ^{98}Mo (values lower than the oceanic input were observed), but rather a shift to lower deep-water $[H_2S]_{aq}$ in the Cape Verde Basin that caused a larger local Mo isotope fractionation between seawater and the sediments (Dickson et al., 2016a). This interpretation is consistent with paleontological and geochemical evidence for cooler and increased oceanic oxygenation during the PCE. Following the PCE, δ^{98}Mo values as high as ~1.4‰ occur in euxinic mudrocks from the Cape Verde Basin, suggesting a return to higher deep-water $[H_2S]_{aq}$ in the basin (Dickson et al., 2016a).

Variations in global seawater δ^{98}Mo during the post-PCE part of OAE2 are difficult to constrain with the available data, as highlighted by the different conclusions reached by Dickson et al. (2016a) and Goldberg et al. (2016) for the same section from the Tarfaya Basin in the proto-North Atlantic Ocean (Fig. 13.4b). Dickson et al. (2016a) used evidence of transient re-oxygenation events (bioturbation, benthic foraminifera) to infer that the Tarfaya Basin was less restricted from the global ocean than the Cape Verde Basin. Hence, a larger local Mo isotope fractionation between seawater and sediments may explain the generally lower δ^{98}Mo in mudrocks of the Tarfaya Basin. By contrast, Goldberg et al. (2016) raised the possibility that rapid fluctuations in seawater δ^{98}Mo between ~0.8 and 1.4‰ were directly captured by Tarfaya Basin euxinic mudrocks (local redox conditions were inferred using Fe speciation) deposited following the PCE. The lowest δ^{98}Mo implies >5% of the global seafloor was covered by euxinic waters. Low Mo/TOC ratios (lower than the Black Sea) in the euxinic mudrocks from the Tarfaya Basin suggest low water column Mo concentrations. Goldberg et al. (2016) suggested that these low Mo/TOC ratios cannot be fully explained solely by the extent of local basin restriction from the open ocean. Instead, an expansion of euxinic seafloor may have caused substantial drawdown of the global oceanic Mo reservoir via Mo removal into euxinic sediments, resulting in low Mo enrichments in the mudrocks. Globally, low Mo/TOC ratios occur in OAE2 mudrocks and suggest a low oceanic Mo inventory (Owens et al., 2016) that may have lowered the oceanic residence time of Mo enough to permit the development of heterogeneous seawater δ^{98}Mo among different ocean basins. This hypothesis may explain the rapid stratigraphic variations in δ^{98}Mo because seawater δ^{98}Mo in local basins would be sensitive to changes in basin restriction, water circulation, and continental runoff (Goldberg et al., 2016).

Distinguishing between these hypotheses is difficult because it is challenging to robustly demonstrate that euxinic mudrocks capture changes in seawater δ^{98}Mo rather than changes in local depositional conditions. We note that it is also possible a global seawater δ^{98}Mo of >1.4‰ occurred during OAE2 because even those samples representing the most intense euxinic conditions locally may have δ^{98}Mo slightly lower than seawater (e.g., Bura-Nakić et al., 2018). Other metal isotope systems are clearly needed to help infer global oceanic redox conditions during OAE2.

Uranium isotope data from sedimentary rocks suggest an expansion of oceanic anoxia/euxinia during OAE2. An initial effort by Montoya Pino et al. (2010) on a small number of organic-rich mudrocks from Demerara Rise (southernmost proto-North Atlantic Ocean) proposed an average negative δ^{238}U excursion of ~0.15‰ for sediments deposited during OAE2 compared with sediments deposited before and after OAE2. A larger sample set of carbonate U isotope data from three localities across OAE2 (Eastbourne and South Ferriby, United Kingdom; Raia del Pedale, Italy) suggested greater variability in global oceanic redox conditions (Clarkson et al., 2018). Consideration was given to the effect of carbonate diagenesis and depositional environment with the pelagic Eastbourne locality interpreted to be better preserved and to capture near-seawater δ^{238}U compositions relative to the pelagic South Ferriby and platformal Raia del Pedale sections. The Eastbourne profile reveals a decrease in δ^{238}U and U/Ca ratios near the onset of OAE2, an increase in δ^{238}U and U/Ca ratios during the PCE, and a decrease in δ^{238}U and U/Ca ratios following the PCE (Fig. 13.5a). The authors interpreted this data, with the aid of a coupled global nutrient cycling model, as representing two expansions of oceanic anoxia separated by a global reoxygenation event coinciding with the PCE. In this framework, the two globally expanded periods of marine anoxia roughly coincided with CO_2 injection into the atmosphere from multiphase LIP volcanism.

Although this interpretation is broadly consistent with Mo isotope trends (cf. Dickson et al. 2016a), we note significant overlap in δ^{238}U (given analytical uncertainties) for the intervals before, during, and after OAE2 as well as between the PCE and the pre- and post-OAE intervals. This overlap may reflect stochastic variations caused by local depositional/diagenetic effects. Hence, the ability of the U isotope proxy to track global oceanic redox changes is limited even for the best-preserved Eastbourne section. The most obvious stratigraphic changes in δ^{238}U occur at the start (increase of ~0.4‰; shift to more oxygenated conditions) and end (decrease of ~0.4‰; shift to more reducing conditions) of the PCE. The shift to lower δ^{238}U

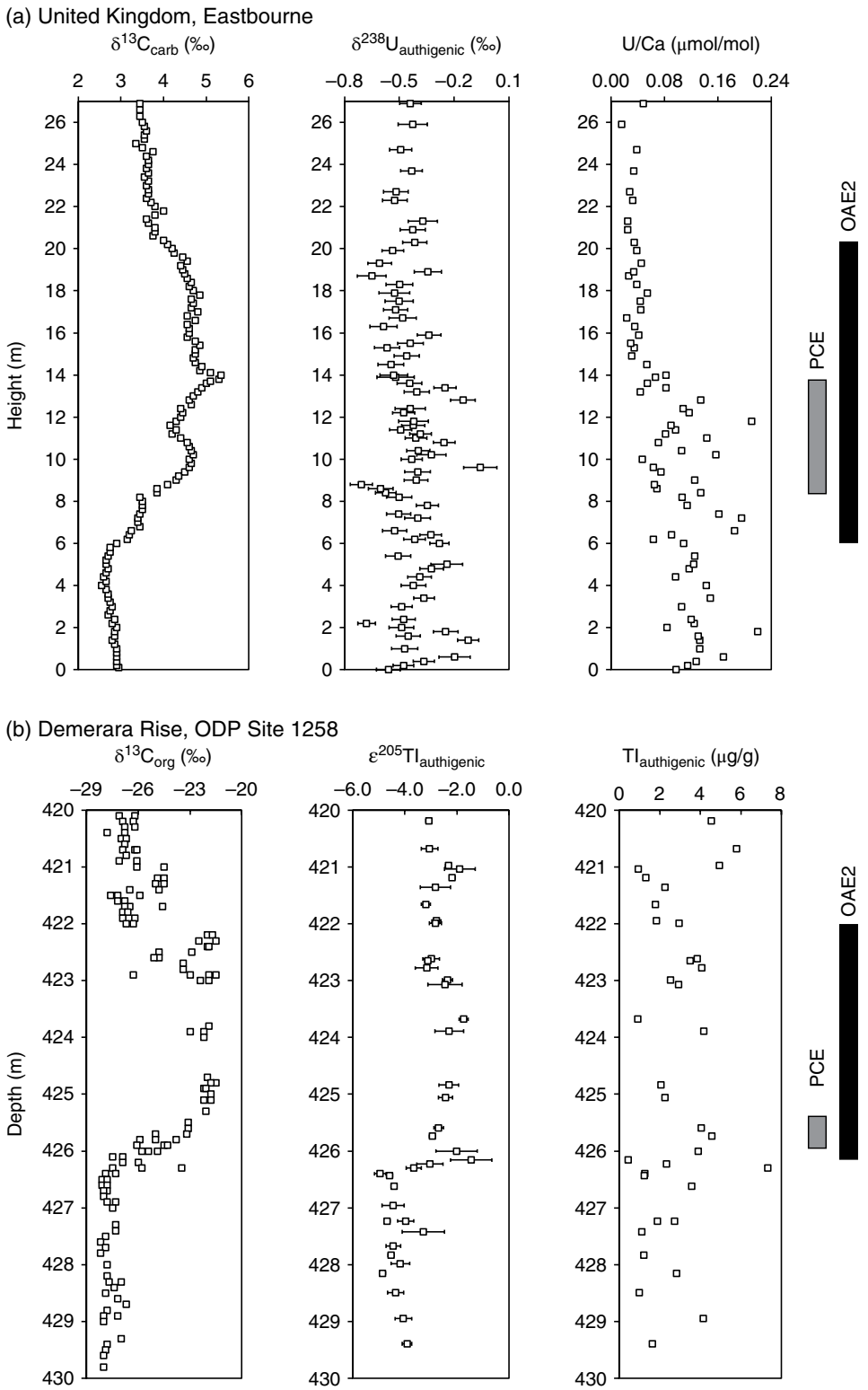

Figure 13.5 Uranium and thallium isotope data for Oceanic Anoxic Event 2 (OAE2). (a) Uranium concentration and uranium isotope data (sodium acetate leachates) for pelagic chalks (foraminiferal-nannofossil carbonate) from the Eastbourne locality, United Kingdom. Data from Clarkson et al. (2018). (b) Thallium concentration and thallium isotope data (2M HNO_3 leachates) for organic-rich mudrocks from Demerara Rise. Data from Ostrander et al. (2017). The positive carbonate (a) and organic (b) carbon isotope excursions marking OAE2 are shown for comparison. PCE = Plenus Cold Event (two discrete intervals for this event have been delineated using paleontological and geochemical data, but for simplicity, a single grey bar is used to denote the event).

at the onset of the CIE is defined by a few samples just prior to the PCE. At the end of the CIE, no clear stratigraphic shift occurs (Clarkson et al., 2018), suggesting global oceanic redox conditions did not significantly change. Mass-balance modeling, which assumes the magnitude of U isotope fractionation is similar for euxinic and anoxic/noneuxinic environments (an assumption currently being scrutinized; see Hood et al., 2016; Cole et al., 2020), suggests 8%–15% anoxic seafloor during OAE2 (Clarkson et al., 2018).

Compared with Mo and U, Tl isotopes offered unique insights into the timing and rate of deoxygenation before, during, and after OAE2. The Tl isotope compositions of organic-rich mudrocks were obtained for two sections from Demerara Rise and the western Tethys, with Fe speciation used to constrain local bottom water redox conditions (Owens et al., 2016, 2017b; Ostrander et al., 2017). At Demerara Rise, a shift in ε^{205}Tl values from ~–5 to ~–2 precedes the positive CIE (Fig. 13.5b). Based on sedimentation rates, this initial Tl isotope perturbation is estimated to occur ~43 ± 11 kyr prior to the beginning of the CIE. Using the mass-balance model of Owens et al. (2017a), the shift to higher ε^{205}Tl suggests a reduction in the extent of well-oxygenated seafloor (where Mn-oxides are buried with an isotopically heavy Tl signature) of ~65%–75% prior to the onset of the CIE. The reduction in Mn oxide burial indicates that sediments overlain by anoxic (noneuxinic and euxinic) and weakly oxygenated bottom waters likely covered or moved over an area more than double the estimated continental margin area during OAE2 (Owens et al., 2018). A similar magnitude of isotopic perturbation was recorded at the western Tethys section (Furlo) despite different and variable local depositional and redox conditions (Owens et al., 2017a; Ostrander et al., 2017). Hence, these sites likely record a global seawater Tl isotopic perturbation. After OAE2 (end of the CIE), the ε^{205}Tl of organic-rich mudrocks remains elevated (–2 to –3), thus indicating that expanded oceanic anoxia continued past the end of the CIE (Ostrander et al., 2017), which is consistent with the U isotope data (Clarkson et al., 2018). Slightly lower ε^{205}Tl in two samples during the PCE may be consistent with a small shift to globally more oxygenated conditions, but additional data are needed to test this hypothesis.

In summary, the Mo, U, and Tl isotope data for OAE2 provided the first detailed constraints on global oceanic redox changes associated with a LIP event. The initial onset of the Tl isotope excursion is within the time estimate for the main phase of LIP activity based on Os isotope variations (Turgeon & Creaser, 2008; Du Vivier et al., 2014, 2015; Ostrander et al., 2017; Dickson et al., Chapter 10 this volume). Trace metal (e.g., Mo, V) depletions in euxinic sediments (reflecting drawdown of the global seawater inventory of these metals; Owens et al., 2016) also suggest an expansion of reducing conditions prior to the onset of the positive CIE. The Mo (Dickson et al., 2016a, b), U (Clarkson et al., 2018), and S (Owens et al., 2013) isotope data indicate an increase in euxinic conditions nearly coincident with the onset of the CIE (Fig. 13.6). Relative to the main phase, there is evidence for earlier but less severe LIP activity (Du Vivier et al., 2014, 2015) but currently, the sampling resolution is not sufficient to observe earlier redox changes. Although these isotope systems probably do not directly respond to LIP magmatism itself, it is likely they do track global redox changes due to the input of reductants, warmer oceans with lower O_2 solubility (triggered by volcanic CO_2 inputs to the atmosphere), and/or increases in primary productivity that drive increased deep-water O_2 consumption (Jenkyns et al., 2017; Clarkson et al., 2018; Them et al., 2018). This globally progressive expansion of anoxic conditions broadly coincides temporally with biological turnover (see Owens et al., 2016). Thus, metal isotopes respond to the environmental deterioration and the cascade of events that LIP activity initiates (Bond & Wignall, 2014; Bryan, Chapter 6 this volume; Bond & Sun, Chapter 3 this volume; Mather & Schmidt, Chapter 4 this volume; Black et al., Chapter 5 this volume; Park et al., Chapter 7 this volume; Youbi et al., Chapter 8 this volume). Metal isotope mass-balance models suggest a spatiotemporal expansion of anoxic and euxinic conditions but also reveal that there was likely still widespread oxic conditions during OAE2.

13.3.2. Toarcian Oceanic Anoxic Event (T-OAE; ~183 Ma)

Molybdenum and thallium isotope data from multiple sections worldwide have been used to track global oceanic redox changes associated with multiple pulses of the Karoo-Ferrar LIP, the Pleinsbachian-Toarcian mass extinction(s), and a pronounced negative CIE that has historically been used to represent the T-OAE.

Molybdenum isotope data from organic-rich mudrocks suggest that an expansion of euxinic marine environments developed in response to the Karoo-Ferrar LIP event (Pearce et al., 2008; Dickson, 2017; Dickson et al., 2017). Compared with OAE2, less geochemical constraints exist for local depositional conditions (i.e., no Fe speciation or U/Mo data) for samples with Mo isotope data. Hence, interpretation of the Mo isotope data is less straightforward although Re/Mo ratios, biomarkers, and the general absence of benthic fossils suggest locally euxinic conditions (at least intermittently) at the studied localities. The TOC-rich mudrocks associated with the negative CIE in the restricted Cleveland Basin (United Kingdom) yield a maximum δ^{98}Mo value of ~1.4‰, which may represent the closest estimate of global seawater δ^{98}Mo and is thus permissive of a similar extent of

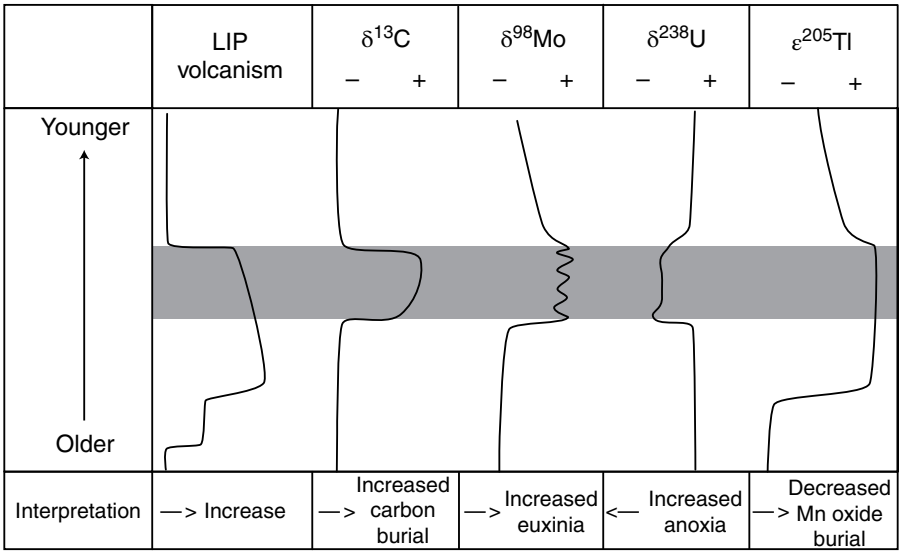

Figure 13.6 A generalized synthesis of changes in global oceanic redox conditions before/during/after LIP events, as inferred from temporal trends in the Mo, U, and Tl isotope compositions of sedimentary rocks across the OAE2, T-OAE, and Permian-Triassic boundary events. Thallium isotopes respond first to deoxygenation associated with the onset of extensive (LIP) volcanic activity because of the shorter oceanic residence time of this metal compared to Mo and U. The global seawater ε^{205}Tl (inferred from organic-rich mudrocks) increases in response to a decrease in the extent of oxygenated seafloor where Mn oxides are buried. The Mo and U isotope records capture an expansion of oceanic euxinia broadly coeval with the onset of the carbon isotope excursion (shown by the grey bar). A decrease in global seawater δ^{238}U can be inferred from a decrease in sedimentary δ^{238}U (carbonates or organic-rich mudrocks). A global expansion of oceanic euxinia is expected to cause a decrease in seawater δ^{98}Mo at the start of the LIP event. However, the observed stratigraphic shift to higher δ^{98}Mo (OAE2, T-OAE) indicates that a change to more intensely reducing conditions at the depositional locality exerted a greater control on stratigraphic changes in δ^{98}Mo than the global expansion of oceanic euxinia. A significant expansion of oceanic euxinia may cause the oceanic residence time of Mo to decrease to the extent that the seawater Mo isotope composition may fluctuate rapidly in response to redox variations or even be spatially heterogeneous among different ocean basins. A positive carbon isotope excursion is shown, reflecting increased organic carbon burial. Some LIP events are associated with a negative carbon isotope excursion that may reflect some combination of greater continental weathering, elevated marine primary productivity, oceanic stratification, and input of isotopically light carbon from LIP volcanism and warming-induced release of methane from sediments, sedimentary rocks, and hydrocarbon deposits (e.g., Zhang et al., 2018b).

euxinic conditions as for OAE2. Lower δ^{98}Mo values for some organic-rich mudrocks during the CIE may not capture global seawater δ^{98}Mo but instead reflect times of decreased drawdown of local aqueous Mo (i.e., nonquantitative Mo removal) because of intermittently less restricted conditions in the Cleveland Basin that would have enabled increased Mo isotope fractionation during Mo burial in sediments. The T-OAE sections from Germany and the Netherlands also have lower δ^{98}Mo than the inferred seawater δ^{98}Mo of ~1.4‰, consistent with less restricted and/or less reducing conditions at those localities. Following the negative CIE, the organic-rich mudrocks have δ^{98}Mo values as high as ~2‰, suggesting a contraction of euxinic marine environments (Pearce et al., 2008; Dickson et al., 2017). The intervals predating the negative CIE have low δ^{98}Mo and are not ideal for inferring global oceanic redox conditions because their low Mo and TOC contents point to locally noneuxinic conditions (Pearce et al., 2008; Dickson et al., 2017).

Two studies have reported the Tl isotope compositions of organic-rich mudrocks associated with the T-OAE from several sections (Nielsen et al., 2011; Them et al., 2018). Nielsen et al. (2011) analyzed two sections (Yorkshire, United Kingdom and Peniche, Portugal) that are likely restricted and, analogous to the Black Sea example, may not capture global seawater ε^{205}Tl (Them et al., 2018). Recently, Them et al. (2018) measured Tl isotopes on euxinic samples (confirmed using Fe speciation) from two well-connected ocean basins, focusing on global oceanic redox changes before the event. The highest resolution section, East Tributary (Western Canada), has pre-CIE ε^{205}Tl baseline values of ~–6 in the Pliensbachian that increase to ~–4 in the earliest Toarcian

(Them et al., 2018). At the onset of the CIE, ε^{205}Tl increases further to values of –2. The initial positive shift in Tl isotopes (to –4) suggests a reduction of Mn oxide burial prior to the T-OAE, similar to that observed for pre-OAE2, but this shift occurs much earlier (~500 kyr) before the CIE compared with OAE2 (~43 kyr). Modeling of this initial shift suggests a 50% reduction in the extent of well-oxygenated seafloor where Mn oxide burial occurs (Owens et al., 2017a; Them et al., 2018). The second positive shift in ε^{205}Tl (to –2) at the onset of the CIE requires an additional 25% reduction of Mn oxide burial (Owens et al., 2017a; Them et al., 2018).

Importantly, the T-OAE is associated with multiphase LIP volcanism (Burgess et al., 2015) and extinction events (as reviewed in Caruthers et al., 2013). The Tl isotope evidence for deoxygenation at times of known LIP volcanism and extinction suggests a causal link. The first pulse of the LIP and initial extinction event nearly coincides with the onset of deoxygenation as recorded by Tl isotopes (Them et al., 2018). The main phase of LIP activity occurs at the onset of the negative CIE with the more severe extinction event and coincides with the most positive ε^{205}Tl, suggesting more widespread anoxic conditions. The Mo isotope data, as well as sulfur isotope compositions from carbonate-associated sulfate (Gill et al., 2011), corroborate this interpretation, suggesting the greatest extent of euxinic conditions occurred during the peak anoxic conditions at the onset of the CIE. Subsequently, the ε^{205}Tl of organic-rich mudrocks decreases to –4, indicating a shift to more oxygenated conditions. Interestingly, the end of the T-OAE (end of the CIE) is marked by higher ε^{205}Tl (–2 to –4), suggesting a continuation of extensive anoxia past the event (Them et al., 2018), with a total duration for expanded oceanic anoxia of >1 Myr. At face value, the Tl isotope data contradicts the Mo isotope evidence for the contraction of euxinic seafloor after the T-OAE. However, this observation may be due to the different response of Mo and Tl to the type of anoxia (euxinia and noneuxinic). Further research is required to resolve this potential discrepancy. The sequence of events before and during T-OAE is generally similar to that observed for OAE2 from the perspective of Tl and Mo isotopes, but the timing, duration, and magnitude vary, which is likely related to the style and magnitude of LIP activity.

13.3.3. End-Permian (~252 Ma)

Molybdenum isotope constraints on oceanic redox conditions for the end-Permian LIP event (Siberian Traps) and associated end-Permian mass extinction are limited to the Sverdrup Basin on the northwest margin of Pangea (Proemse et al., 2013) and the eastern paleo-Tethys Ocean (Chen et al., 2019). Both studies used Mo isotopes to track local ocean redox conditions. Inadequate Mo isotope data exist for demonstrably euxinic samples to robustly evaluate global redox changes during this LIP event. Instead, global oceanic redox changes associated with Siberian Traps LIP emplacement have largely been delineated from stratigraphic trends in the U isotope composition of carbonates (also see Cui et al., Chapter 14 this volume).

Five U isotope studies have been carried out for this event, which represents the most intensive effort to understand LIP-associated oceanic redox changes using a single metal isotope system (Brennecka et al., 2011b; Lau et al., 2016; Elrick et al., 2017; Zhang et al., 2018a, b). Brennecka et al. (2011b) and Lau et al. (2016) observed a significant and sharp decrease in δ^{238}U from –0.3‰ to –0.7‰ in carbonates deposited within the paleo-Tethys ocean around the Permian-Triassic boundary (Dawen and Daijang localities in South China, and Taskent locality in Turkey). This negative δ^{238}U excursion is coeval with the end-Permian mass extinction event and the negative CIE (also see Chen & Xu, Chapter 18 this volume; Cui et al., Chapter 14 this volume; Lounejeva et al., Chapter 16 this volume). The negative δ^{238}U excursion was suggested to capture a decrease in global seawater δ^{238}U caused by an expansion of oceanic anoxia and euxinia (Brennecka et al., 2011b; Lau et al., 2016). Subsequent work by Elrick et al. (2017), Zhang et al. (2018a), and Zhang et al. (2018b) on additional carbonate sections from South China, Japan, and Iran revealed the same sharp decline in δ^{238}U (by >0.5‰ to values as low as about –1.0‰), thus demonstrating that the observed change in δ^{238}U from shallow-water carbonates was a global oceanic signal.

Carbonate U isotope data before, during, and after the end-Permian LIP and mass extinction were used to provide an estimate of the magnitude of global oceanic redox changes. During the Late Permian, global oceanic redox conditions are suggested to have been broadly similar to the modern ocean, with widespread oceanic oxygenation likely prevailing for >1 Myr prior to LIP emplacement and mass extinction (Elrick et al., 2017). Using a U isotope mass balance model, Zhang et al. (2018b) calculated that the areal extent of anoxic seafloor expanded from ~0.2% to ~17-60% in response to LIP activity at the Permian-Triassic boundary. Uranium isotope data also suggest that full biotic recovery from the end-Permian crisis was delayed by ~5 Myr (Lau et al., 2016; Elrick et al., 2017; Zhang et al., 2018b). Multiple negative δ^{238}U and CIE excursions occur at several Early Triassic intervals in the Iranian section. Together with Sr isotope data and modeled seawater phosphate concentrations, these excursions suggest episodes of increased continental weathering and nutrient inputs to the oceans that stimulated primary productivity and expansion of oceanic anoxia (covering ~12%–65% of the seafloor), which may be responsible for elevated

ammonoid extinction rates (Zhang et al., 2018b). These estimates for the extent of seafloor anoxia assumed that global seawater $\delta^{238}U$ was on average ~0.3‰ lower than bulk carbonate $\delta^{238}U$ compositions (like that observed for Bahamian shallow-water platform carbonates; Romaniello et al., 2013; Chen et al., 2018; Tissot et al., 2018).

As noted for OAE2, revised estimates for the extent of seafloor anoxia during the end-Permian LIP event are warranted if the U isotope fractionation in anoxic/noneuxinic environments is smaller than euxinic settings and is closer to oxic/suboxic settings (Hood et al., 2016; Cole et al., 2020). In this scenario, quantitative estimates for the extent of overall oceanic anoxia versus oxygenated seafloor are less straightforward and even ambiguous for some global seawater $\delta^{238}U$ values (notably –0.9‰ to –0.6‰), as shown by the recent U isotope mass-balance model of Gilleaudeau et al. (2019). Nevertheless, this new model suggests that, for global seawater $\delta^{238}U$ of –0.9‰ to –1.0‰, the extent of oceanic euxinia may have reached >10%–20% and was thus likely accompanied by significant noneuxinic anoxia and contracted oceanic oxygenation during the end-Permian evewnt.

13.4. CONCLUSIONS AND FUTURE DIRECTIONS

Redox-sensitive metal isotope systems have strong potential to provide quantitative constraints on global oceanic redox changes in response to LIP volcanic activity. Already, these metal isotope systems have provided novel insights on how LIP events induce environmental change. These initial studies, mostly on the OAE2, T-OAE, and end-Permian events, demonstrate that significant expansion of oceanic anoxia and euxinia (covering an area of seafloor ~1–2 orders of magnitude greater than today) is a consequence of LIP events, with the severity of anoxia and euxinia (and the impact on the biosphere) likely depending on multiple factors, including LIP size/location and the prevailing climate, tectonic, and paleogeographic configuration of continents and oceanic water masses (see Ernst et al., Chapter 1 this volume; Kasbohm et al., Chapter 2 this volume).

Despite the important advances gained in the last decade, precise quantification of the extent of oceanic anoxia for individual LIP events has not been achieved, not even for OAE2, the only event studied using all three metal isotope systems. Such information is required to fully evaluate the role of specific LIP-driven environmental changes on the expansion of oceanic anoxia and euxinia, such as the input of seafloor hydrothermal reductants, temperature-controlled decreases in oceanic O_2 solubility driven by volcanogenic greenhouse gas inputs, and the release of nutrients that stimulate primary productivity and consume deep-ocean O_2. Significant uncertainty in mass-balance model estimates of global oceanic anoxia arises from knowledge gaps in metal isotope fractionation and removal mechanisms in marine environments and challenges associated with inferring seawater metal isotope compositions from sedimentary archives, particularly organic-rich mudrocks. A key focus should be acquisition of Mo, U, and Tl isotope data on the *same* organic-rich mudrock samples (this has not been completed for any LIP interval including OAE2) from time-equivalent sections globally where local depositional conditions are well characterized (e.g., Fe speciation, U/Mo ratios). Application of coupled mass-balance models that also account for higher metal burial fluxes in anoxic/euxinic sediments along continental margin and epeiric seas compared with open-ocean abyssal regions (cf. Reinhard et al., 2013) will enable more accurate estimates for changes in global oceanic redox conditions before, during, and after LIP events. New redox-sensitive metal isotope systems, such as Cr (Holmden et al., 2016; Wang et al., 2016b), V (Wu et al., 2019), and Re (Miller et al., 2015), may provide additional constraints. Organic-rich mudrocks host authigenic enrichments of many redox-sensitive metals, making this sedimentary archive particularly attractive for building large multi-isotope data sets.

There are key Phanerozoic intervals that require further study using multiple metal isotope systems (currently, only a single isotope system has been analyzed in one to two studies for the North Atlantic, Central Atlantic Magmatic Province, and Viluy LIP events; Dickson et al., 2012; Jost et al., 2017; Song et al., 2017; White et al., 2018) or have not yet been studied using Mo, U, or Tl isotopes (Ontong Java Plateau LIP; early Aptian OAE1a). It may also be possible to study global oceanic redox changes associated with Precambrian LIP events using metal isotopes, although the more anoxic conditions prevalent in the oceans at that time (see reviews by Lowenstein et al., 2014; Lyons et al., 2014; Diamond et al., Chapter 21 this volume; Zhang et al., Chapter 20 this volume) may make it challenging to discern LIP-related redox changes. We fully expect that application of metal isotope systems as tracers for redox-related environmental perturbations in the wake of LIP volcanism will continue to accelerate in the coming years. Such research is timely given that climatic changes associated with large atmospheric carbon inputs during LIP events provide insight into the climatic effects of modern anthropogenic disturbance.

ACKNOWLEDGMENTS

The authors declare no conflicts of interest associated with this review paper. François Tissot and two anonymous reviewers are thanked for constructive comments that improved the review paper. B. Kendall acknowledges

funding from the Canada Research Chairs program and a NSERC Discovery Grant (RGPIN-435930). J. Owens acknowledges support from a NASA Exobiology grant (NNX16AJ60G). J. Owens is also supported by the National High Magnetic Field Laboratory (Tallahassee, Florida), which is funded by the National Science Foundation Cooperative Agreement No. DMR1644779 and the State of Florida.

REFERENCES

Algeo, T. J., & Tribovillard, N. (2009). Environmental analysis of paleoceanographic systems based on molybdenum-uranium covariation. *Chemical Geology*, *268,* 211–225.

Andersen, M. B., Elliott, T., Freymuth, H., Sims, K. W. W., Niu, Y., & Kelley, K. A. (2015). The terrestrial uranium isotope cycle. *Nature*, *517,* 356–359.

Andersen, M. B., Matthews, A., Vance, D., Bar-Matthews, M., Archer, C., & de Souza, G. F. (2018). A 10-fold decline in the deep Eastern Mediterranean thermohaline overturning circulation during the last interglacial period. *Earth and Planetary Science Letters*, *503,* 58–67.

Andersen, M. B., Romaniello, S., Vance, D., Little, S. H., Herdman, R., & Lyons, T. W. (2014). A modern framework for the interpretation of $^{238}U/^{235}U$ in studies of ancient ocean redox. *Earth and Planetary Science Letters*, *400,* 184–194.

Andersen, M. B., Stirling, C. H., & Weyer, S. (2017). Uranium isotope fractionation. *Reviews in Mineralogy and Geochemistry*, *82,* 799–850.

Andersen, M. B., Vance, D., Morford, J. L., Bura-Nakić, E., Breitenbach, S. F. M., & Och, L. (2016). Closing in on the marine $^{238}U/^{235}U$ budget. *Chemical Geology*, *420,* 11–22.

Archer, C., & Vance, D. (2008). The isotopic signature of the global riverine molybdenum flux and anoxia in the ancient oceans. *Nature Geoscience, 1*, 597–600.

Arnold, G. L., Anbar, A. D., Barling, J., & Lyons, T. W. (2004). Molybdenum isotope evidence for widespread anoxia in Mid-Proterozoic oceans. *Science*, *304,* 87–90.

Baker, R. G. A., Rehkämper, M., Hinkley, T. K., Nielsen, S. G., & Toutain, J. P. (2009). Investigation of thallium fluxes from subaerial volcanism-Implications for the present and past mass balance of thallium in the oceans. *Geochimica et Cosmochimica Acta*, *73,* 6340–6359.

Barling, J., & Anbar, A. D. (2004). Molybdenum isotope fractionation during adsorption by manganese oxides. *Earth and Planetary Science Letters*, *217,* 315–329.

Barling, J., Arnold, G. L., & Anbar, A. D. (2001). Natural mass-dependent variations in the isotopic composition of molybdenum. *Earth and Planetary Science Letters*, *193,* 447–457.

Bidoglio, G., Gibson, P. N., O'Gorman, M., & Roberts, K. J. (1993). X-ray absorption spectroscopy investigation of surface redox transformations of thallium and chromium on colloidal mineraloxides. *Geochimica et Cosmochimica Acta*, *57,* 2389–2394.

Bond, D. P., & Wignall, P. B. (2014). Large igneous provinces and mass extinctions: an update. *Volcanism, Impacts, and Mass Extinctions: Causes and Effects*, *1*(505), 29–55.

Brennecka, G. A., Herrmann, A. D., Algeo, T. J., & Anbar, A. D. (2011b). Rapid expansion of oceanic anoxia immediately before the end-Permian mass extinction. *Proceedings of the National Academy of Sciences USA*, *108*, 17631–17634.

Brennecka, G. A., Wasylenki, L. E., Bargar, J. R., Weyer, S., & Anbar, A. D. (2011a). Uranium isotope fractionation during adsorption to Mn-oxyhydroxides. *Environmental Science & Technology*, *45*, 1370–1375.

Brown, S. T., Basu, A., Ding, X., Christensen, J. N., & DePaolo, D. J. (2018). Uranium isotope fractionation by abiotic reductive precipitation. *Proceedings of the National Academy of Sciences USA*, *115,* 8688–8693.

Bura-Nakić, E., Andersen, M. B., Archer, C., de Souza, G. F., Marguš, M., & Vance, D. (2018). Coupled Mo-U abundances and isotopes in a small marine euxinic basin: Constraints on processes in euxinic basins. *Geochimica et Cosmochimica Acta*, *222,* 212–229.

Burgess, S. D., Bowring, S. A., Fleming, T. H., & Elliot, D. H. (2015). High-precision geochronology links the Ferrar large igneous province with early-Jurassic ocean anoxia and biotic-crisis. *Earth and Planetary Science Letters*, *415,* 90–99.

Caruthers, A. H., Smith, P. L., & Gröcke, D. R. (2013). The Pliensbachian-Toarcian (Early Jurassic)extinction, a global multi-phased event. *Palaeogeography, Palaeoclimatology, Palaeoecology*, *386,*104–118.

Chen, J., Zhao, L., Algeo, T. J., Zhou, L., Zhang, L., & Qiu, H. (2019). Evaluation of paleomarine redox conditions using Mo-isotope data in low-[Mo] sediments: A case study from the Lower Triassic of South China. *Palaeogeography, Palaeoclimatology, Palaeoecology*, *519,* 178–193.

Chen, X., Romaniello, S. J., Herrmann, A. D., Hardisty, D., Gill, B. C., & Anbar, A. D. (2018). Diagenetic effects on uranium isotope fractionation in carbonate sediments from the Bahamas. *Geochimica et Cosmochimica Acta*, *237,* 294–311.

Clarkson, M. O., Stirling, C. H., Jenkyns, H. C., Dickson, A. J., Porcelli, D., Moy, C. M., Pogge von Strandmann, P. A. E., et al. (2018). Uranium isotope evidence for two episodes of deoxygenation during Oceanic Anoxic Event 2. *Proceedings of the National Academy of Sciences USA*, *115,* 2918–2923.

Cole, D.B., Planavsky, N.J., Longley, M., Böning, P., Wilkes, D., Wang, X., Swanner, E.D., Wittkop, C., Loydell, D., Busigny, V. and Knudsen, A., 2020. Uranium isotope fractionation in non-sulfidic anoxic settings and the global uranium isotope mass balance. Global Biogeochemical Cycles, p.e2020GB006649.

Collier, R. W. (1985). Molybdenum in the Northeast Pacific-Ocean. *Limnology and Oceanography*, *30,* 1351–1354.

Dahl, T. W., Canfield, D. E., Rosing, M. T., Frei, R. E., Gordon, G. W., Knoll, A. H., & Anbar, A. D. (2011). Molybdenum isotope evidence for expansive sulfidic water masses in ~750 Ma oceans. *Earth and Planetary Science Letters, 311,* 264–274.

Dahl, T. W., Chappaz, A., Fitts, J. P., & Lyons, T. W. (2013). Molybdenum reduction in a sulfidic lake: evidence from X-ray absorption fine-structure spectroscopy and implications for the Mo paleoproxy. *Geochimica et Cosmochimica Acta*, *103,* 213–231.

Dahl, T. W., Chappaz, A., Hoek, J., McKenzie, C. J., Svane, S., & Canfield, D. E. (2017). Evidence of molybdenum association with particulate organic matter under sulfidic conditions. *Geobiology*, *15,* 311–323.

Dickson, A. J. (2017). A molybdenum-isotope perspective on Phanerozoic deoxygenation events. Nature Geoscience, 10, 721–726.

Dickson, A. J., Cohen, A. S., & Coe, A. L. (2012). Seawater oxygenation during the Paleocene-Eocene Thermal Maximum. *Geology, 40,* 639–642.

Dickson, A. J., Gill, B. C., Ruhl, M., Jenkyns, H. C., Porcelli, D., Idiz, E., Lyons, T. W., et al. (2017). Molybdenum-isotope chemostratigraphy and paleoceanography of the Toarcian Oceanic Anoxic Event (Early Jurassic). *Paleoceanography*, *32,* 813–829.

Dickson, A. J., Jenkyns, H. C., Porcelli, D., van den Boorn, S., & Idiz, E. (2016a). Basin-scale controls on the molybdenum-isotope composition of seawater during Oceanic Anoxic Event 2 (Late Cretaceous). *Geochimica et Cosmochimica Acta*, *178,* 291–306.

Dickson, A. J., Jenkyns, H. C., Porcelli, D., van den Boorn, S., Idiz, E., & Owens, J. D. (2016b). Corrigendum to "Basin-scale controls on the molybdenum-isotope composition of seawater during Oceanic Anoxic Event 2 (Late Cretaceous)" [*Geochimica et Cosmochimica Acta* (2016), *178,* 291–306]. *Geochimica et Cosmochimica Acta*, *189,* 404–405.

Dunk, R. M., Mills, R. A., & Jenkins, W. J. (2002). A reevaluation of the oceanic uranium budget for the Holocene. *Chemical Geology*, *190,* 45–67.

Du Vivier, A. D. C., Selby, D., Condon, D. J., Takashima, R., & Nishi, H. (2015). Pacific $^{187}Os/^{188}Os$ isotope chemistry and U-Pb geochronology: Synchroneity of global Os isotope change across OAE2. *Earth and Planetary Science Letters*, *428,* 204–216.

Du Vivier, A. D. C., Selby, D., Sageman, B. B., Jarvis, I., Gröcke, D. R., & Voigt, S. (2014). Marine $^{187}Os/^{188}Os$ isotope stratigraphy reveals the interaction of volcanism and ocean circulation during Oceanic Anoxic Event 2. *Earth and Planetary Science Letters*, *389,* 23–33.

Elrick, M., Polyak, V., Algeo, T. J., Romaniello, S., Asmerom, Y., Herrmann, A. D., Anbar, A. D., et al. (2017). Global-ocean redox variation during the middle-late Permian through Early Triassic based on uranium isotope and Th/U trends of marine carbonates. *Geology*, *45,* 163–166.

Erickson, B. E., & Helz, G. R. (2000). Molybdenum (VI) speciation in sulfidic waters: stability and lability of thiomolybdates. *Geochimica et Cosmochimica Acta*, *64,* 1149–1158.

Fan, H., Nielsen, S. G., Owens, J. D., Auro, M., Shu, Y., Hardisty, D. S., Horner, T. J., Bowman, C. N., Young, S. A., & Wen, H. (2020). Constraining oceanic oxygenation during the Shuram excursion in South China using thallium isotopes. Geobiology, 18, 348–365.

Gill, B. C., Lyons, T. W., & Jenkyns, H. C. (2011). A global perturbation to the sulfur cycle duringthe Toarcian oceanic anoxic event. *Earth and Planetary Science Letters*, *312,* 484–496.

Gilleaudeau, G. J., Romaniello, S. J., Luo, G., Kaufman, A. J., Zhang, F., Klaebe, R. M., Kah, L.C., et al. (2019). Uranium isotope evidence for limited euxinia in mid-Proterozoic oceans. *Earth and Planetary Science Letters*, *521,* 150–157.

Goldberg, T., Archer, C., Vance, D., Thamdrup, B., McAnena, A., & Poulton, S. W. (2012). Controls on Mo isotope fractionations in a Mn-rich anoxic marine sediment, Gullmar Fjord, Sweden. *Chemical Geology*, *296–297,* 73–82.

Goldberg, T., Poulton, S. W., Wagner, T., Kolonic, S. F., & Rehkämper, M. (2016). Molybdenum drawdown during Cretaceous Oceanic Anoxic Event 2. *Earth and Planetary Science Letters*, *440,* 81–91.

Goto, K. T., Anbar, A. D., Gordon, G. W., Romaniello, S. J., Shimoda, G., Takaya, Y., Tokumaru, A., et al. (2014). Uranium isotope systematics of ferromanganese crusts in the Pacific Ocean: Implications for the marine $^{238}U/^{235}U$ isotope system. *Geochimica et Cosmochimica Acta*, *146,* 43–58.

Helz, G. R., & Vorlicek, T. P. (2019). Precipitation of molybdenum from euxinic waters and the role of organic matter. *Geochimica et Cosmochimica Acta*, *509,* 178–193.

Helz, G. R., Miller, C. V., Charnock, J. M., Mosselmans, J. F. W., Pattrick, R. A. D., Garner, C. D., & Vaughan, D. J. (1996). Mechanism of molybdenum removal from the sea and its concentration in black shales: EXAFS evidence. *Geochimica et Cosmochimica Acta*, *60,* 3631–3642.

Holmden, C., Amini, M., & Francois, R. (2015). Uranium isotope fractionation in Saanich Inlet: A modern analog study of a paleoredox tracer. *Geochimica et Cosmochimica Acta*, *153,* 202–215.

Holmden, C., Jacobson, A. D., Sageman, B. B., & Hurtgen, M. T. (2016). Response of the Cr isotope proxy to Cretaceous Oceanic Anoxic Event 2 in a pelagic carbonate succession from the Western Interior Seaway. *Geochimica et Cosmochimica Acta*, *186,* 277–295.

Hood, A. V. S., Planavsky, N. J., Wallace, M. W., Wang, X., Bellefroid, E. J., Gueguen, B., & Cole, D. B. (2016). Integrated geochemical-petrographic insights from component-selective $\delta^{238}U$ of Cryogenian marine carbonates. *Geology, 44,* 935–938.

Jenkyns, H. C., Dickson, A. J., Ruhl, M., & Van Den Boorn, S. H. J. M. (2017). Basalt-seawater interaction, the Plenus Cold Event, enhanced weathering and geochemical change: Deconstructing Oceanic Anoxic Event 2 (Cenomanian-Turonian, Late Cretaceous). *Sedimentology*, *64,* 16–43.

Jost, A. B., Bachan, A., van de Schootbrugge, B., Lau, K. V., Weaver, K. L., Maher, K., & Payne, J. L. (2017). Uranium isotope evidence for an expansion of marine anoxia during the end-Triassic extinction. *Geochemistry, Geophysics, Geosystems*, *18,* 3093–3108.

Kendall, B., Dahl, T. W., & Anbar, A. D. (2017). Good golly, why moly? The s isotope geochemistry of molybdenum. *Reviews in Mineralogy and Geochemistry*, *82,* 683–732.

King, E. K., & Pett-Ridge, J. C. (2018). Reassessing the dissolved molybdenum isotopic composition of ocean inputs: The effect of chemical weathering and groundwater. *Geology*, *46,* 955–958.

Lau, K. V., Maher, K., Altiner, D., Kelley, B. M., Kump, L. R., Lehrmann, D. J., Silva-Tamayo, J. C., et al. (2016). Marine anoxia and delayed Earth system recovery after the end-Permian extinction. *Proceedings of the National Academy of Sciences USA*, *113,* 2360–2365.

Lowenstein, T. K., Kendall, B., & Anbar, A. D. (2014). The geologic history of seawater. In H. D. Holland, & K. K. Turekian (Eds.), *Treatise on geochemistry: Second edition; Volume 8, The oceans and marine geochemistry* (pp. 569–622). Elsevier Inc.

Lyons, T. W., Reinhard, C. T., & Planavsky, N. J. (2014). The rise of oxygen in Earth's early ocean and atmosphere. *Nature*, *506,* 307–315.

Miller, C. A., Peucker-Ehrenbrink, B., & Schauble, E. A. (2015). Theoretical modeling of rhenium isotope fractionation, natural variations across a black shale weathering profile, and potential as a paleoredox proxy. *Earth and Planetary Science Letters*, *430,* 339–348.

Miller, C. A., Peucker-Ehrenbrink, B., Walker, B. D., & Marcantonio, F. (2011). Re-assessing the surface cycling of molybdenum and rhenium. *Geochimica et Cosmochimica Acta*, *75,* 7146–7179.

Montoya-Pino, C., Weyer, S., Anbar, A. D., Pross, J., Oschmann, W., van de Schootbrugge, B., & Arz, H. W. (2010). Global enhancement of ocean anoxia during Oceanic Anoxic Event 2: A quantitative approach using U isotopes. *Geology*, *38,* 315–318.

Morford, J. L., & Emerson, S. (1999). The geochemistry of redox sensitive trace metals in sediments. *Geochimica et Cosmochimica Acta*, *63,* 1735–1750.

Nägler, T. F., Anbar, A. D., Archer, C., Goldberg, T., Gordon, G. W., Greber, N. D., Siebert, C., et al. (2014). Proposal for an international molybdenum isotope measurement standard and data representation. *Geostandards and Geoanalytical Research*, *38,* 149–151.

Nägler, T. F., Neubert, N., Böttcher, M. E., Dellwig, O., & Schnetger, B. (2011). Molybdenum isotope fractionation in pelagic euxinia: Evidence from the modern Black and Baltic Seas. *Chemical Geology*, *289,* 1–11.

Nakagawa, Y., Takano, S., Firdaus, M. L., Norisuye, K., Hirata, T., Vance, D., & Sohrin, Y. (2012). The molybdenum isotopic composition of the modern ocean. *Geochemical Journal*, *46,* 131–141.

Neely, R. A., Gislason, S. R., Ólafsson, M., McCoy-West, A. J., Pearce, C. R., & Burton, K. W. (2018). Molybdenum isotope behavior in groundwaters and terrestrial hydrothermal systems, Iceland. *Earth and Planetary Science Letters, 486,* 108–118.

Neubert, N., Nägler, T. F., & Böttcher, M. E. (2008). Sulfidity controls molybdenum isotope fractionation onto euxinic sediments: Evidence from the modern Black Sea. *Geology, 36,* 775–778.

Nielsen, S. G., Goff, M., Hesselbo, S. P., Jenkyns, H. C., LaRowe, D. E., & Lee, C.-T. A. (2011). Thallium isotopes in early diagenetic pyrite – a paleoredox proxy? *Geochimica et Cosmochimica Acta*, *75,* 6690–6704.

Nielsen, S. G., Klein, F., Kading, T., Blusztajn, J., & Wickham, K. (2015). Thallium as a tracer of fluid-rock interaction in the shallow Mariana forearc. *Earth and Planetary Science Letters*, *430,* 416–426.

Nielsen, S. G., Mar-Gerrison, S., Gannoun, A., LaRowe, D., Klemm, V., Halliday, A. N., Burton, K. W., et al. (2009). Thallium isotope evidence for a permanent increase in marine organic carbon export in the early Eocene. *Earth and Planetary Science Letters*, *278,* 297–307.

Nielsen, S. G., Rehkämper, M., & Prytulak, J. (2017). Investigation and application of thallium isotope fractionation. *Reviews in Mineralogy and Geochemistry*, *82,* 759–798.

Nielsen, S. G., Rehkämper, M., Norman, M. D., Halliday, A. N., & Harrison, D. (2006b). Thallium isotopic evidence for ferromanganese sediments in the mantle source of Hawaiian basalts. *Nature*, *439,* 314–317.

Nielsen, S. G., Rehkämper, M., Porcelli, D., Andersson, P. S., Halliday, A. N., Swarzenski, P. W., Latkoczy, C., et al. (2005). The thallium isotope composition of the upper continental crust and rivers: An investigation of the continental sources of dissolved marine thallium. *Geochimica et Cosmochimica Acta*, *69,* 2007–2019.

Nielsen, S. G., Rehkämper, M., Teagle, D. A., Butterfield, D. A., Alt, J. C., & Halliday, A. N. (2006a). Hydrothermal fluid fluxes calculated from the isotopic mass balance of thallium in the ocean crust. *Earth and Planetary Science Letters*, *251,* 120–133.

Nielsen, S. G., Wasylenki, L. E., Rehkämper, M., Peacock, C. L., Xue, Z., & Moon, E. M. (2013). Towards an understanding of thallium isotope fractionation during adsorption to manganese oxides. *Geochimica et Cosmochimica Acta*, *117,* 252–265.

Noordmann, J., Weyer, S., Georg, R. B., Jons, S., & Sharma, M. (2016) $^{238}U/^{235}U$ isotope ratios of crustal material, rivers and products of hydrothermal alteration: New insights on the oceanic U isotope mass balance. *Isotopes in Environmental and Health Studies, 52,* 141–163.

Noordmann, J., Weyer, S., Montoya-Pino, C., Dellwig, O., Neubert, N., Eckert, S., Paetzel, M., et al. (2015). Uranium and molybdenum isotope systematics in modern euxinic basins: Case studies from the central Baltic Sea and the Kyllaren fjord (Norway). *Chemical Geology*, *396,* 182–195.

Ostrander, C. M., Owens, J. D., & Nielsen, S. G. (2017). Constraining the rate of oceanic deoxygenation leading up to a Cretaceous Oceanic Anoxic Event (OAE-2: ~94 Ma). *Science Advances*, *3,* e1701020.

Owens, J. D., Gill, B. C., Jenkyns, H. C., Bates, S. M., Severmann, S., Kuypers, M. M. M., Woodfine, R. G., et al. (2013). Sulfur isotopes track the global extent and dynamics of euxinia during Cretaceous Oceanic Anoxic Event 2. *Proceedings of the National Academy of Sciences U.S.A.*, *110,* 18407–18412.

Owens, J. D., Lyons, T. W., & Lowery, C. M. (2018). Quantifying the missing sink for global organic carbon burial during a Cretaceous oceanic anoxic event. *Earth and Planetary Science Letters*, *499,* 83–94.

Owens, J. D., Lyons, T. W., Hardisty, D. S., Lowery, C. M., Lu, Z., Lee, B., & Jenkyns, H. C., (2017b). Patterns of local and global redox variability during the Cenomanian–Turonian Boundary Event (Oceanic Anoxic Event 2) recorded in carbonates and shales from central Italy. *Sedimentology*, *64,* 168–185.

Owens, J. D., Niesen, S. G., Horner, T. J., Ostrander, C. M., & Peterson, L. C. (2017a). Thallium-isotopic compositions of euxinic sediments as a proxy for global manganese-oxide burial. *Geochimica et Cosmochimica Acta*, *213,* 291–307.

Owens, J. D., Reinhard, C. T., Rohrssen, M., Love, G. D., & Lyons, T. W. (2016). Empirical links between trace metal cycling and marine microbial ecology during a large perturbation to Earth's carbon cycle. *Earth and Planetary Science Letters*, *449,* 407–417.

Peacock, C. L., & Moon, E. M. (2012). Oxidative scavenging of thallium by birnessite: Explanation for thallium enrichment and stable isotope fractionation in marine ferromanganese precipitates. *Geochimica et Cosmochimica Acta*, *84,* 297–313.

Pearce, C. R., Cohen, A. S., Coe, A. L., & Burton, K. W. (2008). Molybdenum isotope evidence for global ocean anoxia coupled with perturbations to the carbon cycle during the Early Jurassic. *Geology*, *36,* 231–234.

Poulson, R. L., Siebert, C., McManus, J., & Berelson, W. M. (2006). Authigenic molybdenum isotope signatures in marine sediments. *Geology*, *34,* 617–620.

Poulson Brucker, R. L., McManus, J., & Poulton, S. W. (2012). Molybdenum isotope fractionations observed under anoxic experimental conditions. *Geochemical Journal*, *46,* 201–209.

Poulson Brucker, R. L., McManus, J., Severmann, S., & Berelson, W. M. (2009). Molybdenum behavior during early diagenesis: Insights from Mo isotopes. *Geochemistry, Geophysics, Geosystems*, *10,* Q06010.

Proemse, B. C., Grasby, S. E., Wieser, M. E., Mayer, B., & Beauchamp, B. (2013). Molybdenum isotopic evidence for oxic marine conditions during the latest Permian extinction. *Geology*, *41,* 967–970.

Rehkämper, M., & Nielsen, S. G. (2004). The mass balance of dissolved thallium in the oceans. *Marine Chemistry*, *85,* 125–139.

Rehkämper, M., Frank, M., Hein, J. R., & Halliday, A. (2004). Cenozoic marine geochemistry of thallium deduced from isotopic studies of ferromanganese crusts and pelagic sediments. *Earth and Planetary Science Letters*, *219,* 77–91.

Rehkämper, M., Frank, M., Hein, J. R., Porcelli, D., Halliday, A., Ingri, J., & Liebetrau, V. (2002). Thallium isotope variations in seawater and hydrogenetic, diagenetic, and hydrothermal ferromanganese deposits. *Earth Planetary Science Letters*, *197,* 65–81.

Reinhard, C. T., Planavsky, N. J., Robbins, L. J., Partin, C. A., Gill, B. C., Lalonde, S. V., Bekker, A., et al. (2013). Proterozoic ocean redox and biogeochemical stasis. *Proceedings of the National Academy of Sciences USA*, *110,* 5357–5362.

Rolison, J. M., Stirling, C. H., Middag, R., & Rijkenberg, M. J. A. (2017). Uranium stable isotope fractionation in the Black Sea: Modern calibration of the $^{238}U/^{235}U$ paleo-redox proxy. *Geochimica et Cosmochimica Acta*, *203,* 69–88.

Romaniello, S. J., Herrmann, A. D., & Anbar, A. D. (2013). Uranium concentrations and $^{238}U/^{235}U$ isotope ratios in modern carbonates from the Bahamas: assessing a novel paleoredox proxy. *Chemical Geology*, *362,* 305–316.

Rue, E. L., Smith, G. J., Cutter, G. A., & Bruland, K. W. (1997). The response of trace element redox couples to suboxic conditions in the water column. *Deep Sea Research Part I*, *44,* 113–134.

Sarmiento, J. L., & Gruber, N. (2006). *Ocean biogeochemical dynamics*. New Jersey: Princeton University Press.

Scholz, F., Baum, M., Siebert, C., Eroglu, S., Dale, A. W., Naumann, M., & Sommer, S. (2018). Sedimentary molybdenum cycling in the aftermath of seawater inflow to the intermittently euxinic Gotland Deep, Central Baltic Sea. *Chemical Geology*, *491*, 27–38.

Scott, C., & Lyons, T. W. (2012). Contrasting molybdenum cycling and isotopic properties in euxinic versus non-euxinic sediments and sedimentary rocks: Refining the paleoproxies. *Chemical Geology*, *324–325,* 19–27.

Scott, C., Lyons, T. W., Bekker, A., Shen, Y., Poulton, S. W., Chu, X., & Anbar, A. D. (2008). Tracing the stepwise oxygenation of the Proterozoic ocean. *Nature*, *452*, 456–459.

Siebert, C., McManus, J., Bice, A., Poulson, R., & Berelson, W. M. (2006). Molybdenum isotope signatures in continental margin marine sediments. *Earth and Planetary Science Letters*, *241*, 723–733.

Siebert, C., Nägler, T. F., von Blanckenburg, F., & Kramers, J. D. (2003). Molybdenum isotope records as a potential new proxy for paleoceanography. *Earth and Planetary Science Letters*, *211*, 159–171.

Song, H., Song, H., Algeo, T. J., Tong, J., Romaniello, S. J., Zhu, Y., Chu, D., et al. (2017). Uranium and carbon isotopes document global-ocean redox-productivity relationships linked to cooling during the Frasnian-Famennian mass extinction. *Geology*, *45*, 887–890.

Stirling, C. H., Andersen, M. B., Potter, E.-M., & Halliday, A. N. (2007). Low-temperature isotopic fractionation of uranium. *Earth and Planetary Science Letters*, *264*, 208–225.

Stylo, M., Neubert, N., Wang, Y., Monga, N., Romaniello, S. J., Weyer, S., & Bernier-Latmani, R. (2015). Uranium isotopes fingerprint biotic reduction. *Proceedings of the National Academy of Sciences USA*, *112*, 5619–5624.

Them, T. R., Gill, B. C., Caruthers, A. H., Gerhardt, A. M., Gröcke, D. R., Lyons, T. W., Marroquín, S. M., et al. (2018). Thallium isotopes reveal protracted anoxia during the Toarcian (Early Jurassic) associated with volcanism, carbon burial, and mass extinction. *Proceedings of the National Academy of Sciences USA*, *115*, 6596–6601.

Tissot, F. L., Chen, C., Go, B. M., Naziemiec, M., Healy, G., Bekker, A., Swart, P. K., et al. (2018). Controls of eustasy and diagenesis on the $^{238}U/^{235}U$ of carbonates and evolution of the seawater ($^{234}U/^{238}U$) during the last 1.4 Myr. *Geochimica et Cosmochimica Acta*, *242*, 233–265.

Tissot, F. L. H., & Dauphas, N. (2015). Uranium isotopic compositions of the crust and ocean: age corrections, U budget and global extent of modern anoxia. *Geochimica et Cosmochimica Acta*, *167*, 113–143.

Turgeon, S. C., & Creaser, R. A. (2008) Cretaceous oceanic anoxic event 2 triggered by a massive magmatic episode. *Nature*, *454*, 323–326.

Wang, X., Planavsky, N. J., Reinhard, C. T., Hein, J. R., & Johnson, T. M. (2016a). A Cenozoic seawater redox record derived from $^{238}U/^{235}U$ in ferromanganese crusts. *American Journal of Science*, *316*, 64–83.

Wang, X., Reinhard, C. T., Planavsky, N. J., Owens, J. D., Lyons, T. W., & Johnson, T. M. (2016b). Sedimentary chromium isotopic compositions across the Cretaceous OAE2 at Demarara Rise Site 1258. *Chemical Geology*, *429*, 85–92.

Wasylenki, L. E., Rolfe, B. A., Weeks, C. L., Spiro, T. G., & Anbar, A. D. (2008). Experimental investigation of the effects of temperature and ionic strength on Mo isotope fractionation during adsorption to manganese oxides. *Geochimica et Cosmochimica Acta*, *72*, 5997–6005.

Westermann, S., Vance, D., Cameron, V., Archer, C., & Robinson, S. A. (2014). Heterogeneous oxygenation states in the Atlantic and Tethys oceans during Oceanic Anoxic Event 2. *Earth and Planetary Science Letters*, *404*, 178–189.

Weyer, S., Anbar, A. D., Gerdes, A., Gordon, G. W., Algeo, T. J., & Boyle, E. A. (2008). Natural fractionation of $^{238}U/^{235}U$. *Geochimica et Cosmochimica Acta*, *72*, 345–359.

Wheat, C. G., Mottl, M. J., & Rudnicki, M. (2002). Trace element and REE composition of a low-temperature ridge-flank hydrothermal spring. *Geochimica et Cosmochimica Acta*, *66,* 3693–3705.

White, D. A., Elrick, M., Romaniello, S., & Zhang, F. (2018). Global seawater redox trends during the Late Devonian mass extinction detected using U isotopes of marine limestones. *Earth and Planetary Science Letters*, *503*, 68–77.

Willbold, M., & Elliot, T. (2017). Molybdenum isotope variations in magmatic rocks. *Chemical Geology*, *449*, 253–268.

Wu, F., Owens, J. D., Huang, T., Sarafian, A., Huang, K.–F., Sen, I. S., Horner, T. J., et al. (2019). Vanadium isotope composition of seawater. *Geochimica et Cosmochimica Acta*, *244*, 403–415.

Yang, J., Siebert, C., Barling, J., Savage, P., Liang, Y.-H., & Halliday, A. N. (2015). Absence of molybdenum isotope fractionation during magmatic differentiation at Hekla volcano, Iceland. *Geochimica et Cosmochimica Acta*, *162*, 126–136.

Zhang, F., Algeo, T. J., Romaniello, S. J., Cui, Y., Zhao, L., Chen, Z.-Q., & Anbar, A. D. (2018a). Congruent Permian-Triassic $\delta^{238}U$ records at Panthalassic and Tethyan sites: Confirmation of global-oceanic anoxia and validation of the U-isotopic paleoredox proxy. *Geology*, *46*, 327–330.

Zhang, F., Romaniello, S. J., Algeo, T. J., Lau, K. V., Clapham, M. E., Richoz, S., Herrmann, A. D., et al. (2018b). Multiple episodes of extensive marine anoxia linked to global warming and continental weathering following the latest Permian mass extinction. *Science Advances*, *4*, e1602921.